

Copyright © 1997, by the author(s).
All rights reserved.

Permission to make digital or hard copies of all or part of this work for personal or classroom use is granted without fee provided that copies are not made or distributed for profit or commercial advantage and that copies bear this notice and the full citation on the first page. To copy otherwise, to republish, to post on servers or to redistribute to lists, requires prior specific permission.

CONTROL OF A TELESURGICAL WORKSTATION

by

Murat Cenk Cavuřoglu

Memorandum No. UCB/ERL M97/35

20 May 1997

CONTROL OF A TELESURGICAL WORKSTATION

Copyright © 1997

by

Murat Cenk Cavuşoğlu

Memorandum No. UCB/ERL M97/35

20 May 1997

ELECTRONICS RESEARCH LABORATORY

College of Engineering
University of California, Berkeley
94720

Abstract

Control of a Telesurgical Workstation

by

Murat Cenk Çavuşoğlu

Master of Science, Plan II in Department of Electrical Engineering and Computer
Sciences

University of California at Berkeley

Professor S. Shankar Sastry, Chair

Medical robotics and computer aided surgery in general, and robotic telesurgery in particular, are promising applications of robotics. In this report, various aspects of telesurgery are studied. After a general introduction to laparoscopic surgery and medical applications of robotics, in the first part, the Berkeley/UCSF Telesurgical Workstation, a master-slave telerobotic system for laparoscopic surgery, is introduced, followed by its kinematic analysis and discussion on its control. In the second part, conceptual and future issues on telesurgery are studied in detail, including discussions on teleoperation, hybrid control and visualization. Discussions on teleoperation introduce the fidelity-stability trade-off in teleoperation systems, give a general overview of the control algorithms present in the literature, and discuss the special requirements of telesurgery. Hybrid control is used to design the least restrictive control law for the telesurgical robot to limit the interaction forces for guaranteed safe operation. The visualization section discusses the general problems of the display system used in laparoscopic surgery, and proposes ways to overcome them, with a case study on 3D surface reconstruction from camera motion in laparoscopic images.

Dedicated to my family...

Contents

List of Figures	vi
List of Tables	vii
1 Introduction	1
I Berkeley/UCSF Telesurgical Workstation	4
2 Description of the System	5
3 Kinematics	9
3.1 Slave Manipulator Inverse Kinematics	9
3.1.1 Serial Part	10
3.1.2 Parallel Part	12
3.2 Master Manipulator Forward Kinematics	17
4 Control	20
4.1 Open Loop Issues	20
4.2 Control Algorithm	21
4.3 Discussion	21
II Conceptual and Future Issues in Telesurgery	23
5 Teleoperation for Telesurgery	24
5.1 Basic Issues — Stability-Fidelity Trade-off	24
5.1.1 Analysis with Network Equivalents and Two-Port Models	25
5.2 Control Algorithms Overview	27
5.2.1 Control Algorithms	28
5.2.2 Experimental Comparison of Algorithms in Conventional Teleopera- tion Tasks	31
5.3 Discussion in the Context of Telesurgery	32

6	Hybrid Control	34
6.1	Game Theory Approach to Hybrid Control Design	34
6.2	Controller Design for One DOF Manipulator	35
6.2.1	Case 1: $\dot{x}(0) > 0$	36
6.2.2	Case 2: $\dot{x}(0) < 0$	37
6.2.3	Simulation Results	38
6.3	Extension to Multi DOF Manipulators	40
6.4	Discussion	43
7	Visualization Issues in Telesurgery	44
7.1	Case Study: 3D Surface Reconstruction from Camera Motion in Laparoscopic Images	45
8	Conclusion and Future Directions	51
	Bibliography	53

List of Figures

1.1	4 DOF available in conventional laparoscopic instruments	2
2.1	Slave manipulator of the Berkeley/UCSF laparoscopic workstation	7
2.2	Master manipulator of the Berkeley/UCSF laparoscopic workstation	8
2.3	Close-up view of the master manipulator	8
3.1	Parallel and serial parts of the slave robot	10
3.2	Naming convention and the zero configuration of the serial part	11
3.3	Kinematic diagram of the side view of parallel section	13
3.4	Naming convention and the zero configuration of the master manipulator	17
4.1	Yaw sensor input-output characteristic	21
4.2	Control system block diagram	22
4.3	Current implementation of master-slave control	22
5.1	Master-slave system representation	25
5.2	Master-slave system coupled with operator and environment	27
5.3	Block diagram of a typical 6 DOF position control based algorithm	28
5.4	Remote site compliance	29
5.5	Kinesthetic force feedback	29
5.6	Position error based force feedback	30
5.7	Block diagram of a passive communication block	30
6.1	1 DOF contact model	35
6.2	Approach phase simulation	39
6.3	In-contact motion simulation	40
6.4	2 DOF manipulator model	41
7.1	Cross-section of a laparoscope	45
7.2	Epipolar lines for calculation points	49
7.3	Epipolar lines for test points	49
7.4	Calculated depth map	50

List of Tables

2.1	Performance goals for the millirobot	6
2.2	Millirobot test results	6
2.3	Performance goals for the second version of the millirobot	6

Acknowledgements

I would like to express my sincere appreciations to my advisor Prof. S. Shankar Sastry, for his invaluable support and advise, and to Prof. Frank Tendick, for his help and guidance at every step of my research. I also would like to thank to Prof. Fearing for the advice he provided.

I am also grateful to Joseph Yan, who was a research partner in parts of this work, and also to John Koo, for his fruitful comments throughout the time.

Last, but not the least, I want to express my thanks to my parents, who encouraged and helped me to pursue my dreams in this *New World*.

This research would not have been accomplished without the generous financial support from the National Science Foundation under grant IRI-95-31837, the Office of Naval Research under grant MURI N14-96-1-1200, and the National Aeronautics and Space Administration under STTR grant NAS1-20288.

Chapter 1

Introduction

Medical robotics and computer assisted surgery are new and promising fields of study, which aim to augment the capabilities of surgeons by taking the best from robots and humans.

In joint project between the Robotics and Intelligent Machines Laboratory of University of California at Berkeley, and the Department of Surgery of University of California at San Francisco, a telesurgical workstation is being developed for use in laparoscopic surgery [34]. The current design is a 6 DOF manipulator instrumented with a gripper controlled by a 6 DOF master manipulator.

Research on medical robotics at UC Berkeley includes (but is not limited to) the development of an endoscopic manipulator, early designs of millirobotic manipulators for laparoscopy [45, 44, 8], and studies on tactile sensing [9, 16].

What is Laparoscopic Surgery?

Laparoscopic surgery, or more generally endoscopic surgery, is a revolutionary technique in surgery.¹ They are minimally invasive, i.e. the operation is performed with instruments inserted through small incisions ($\sim 10\text{mm}$ in diameter) rather than by making a large incision to expose the operation site. The main advantage of this technique is the reduced trauma to healthy tissue, which is the major reason for post-operational pain and long hospital stay of the patient. The hospital stay and rest periods, and therefore the operations' cost, are significantly reduced with minimally invasive operations, at the

¹For an in-depth treatment of laparoscopic surgery refer to [43]

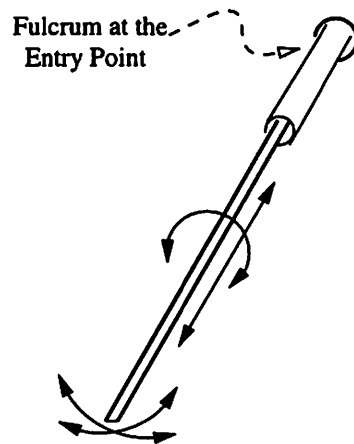


Figure 1.1: 4 DOF available in conventional laparoscopic instruments

expense of more difficult techniques performed by the surgeon.

Minimally invasive operations include laparoscopy (abdominal cavity), thoracoscopy (chest cavity), arthroscopy (joints), pelviscopy (pelvis), and angioscopy (blood vessels). The first laparoscopic surgery was performed in 1985 by Mühe in (West) Germany. In the last decade, there was a quick shift from open surgery to laparoscopic surgery in simple operations, the most dramatic one being cholecystectomy (removal of gallbladder), of which 67% were performed laparoscopically in the US in 1993 [15].

In laparoscopic surgery, the abdominal cavity, which is expanded by pumping carbon dioxide inside to open a workspace, is observed with a laparoscope inserted through one of the incisions. The laparoscope itself is composed of a chain of lens optics to transmit the image of the operation site to the CCD camera connected to its outer end, and fiber optic cables to carry light to illuminate inside (see chapter 7 for an illustration and more information). A monoscopic image of the operation site is displayed on a TV screen. The instruments used for the operation are specially designed long and thin instruments and they are inserted through trocars put at the incision to air seal the abdomen. The instruments have only 4 DOF (see figure 1.1), preventing the ability to arbitrarily orient the instrument tip, and trigger-like handles. The dexterity is significantly reduced because of the lost DOF's and motion reversal due to the fulcrum at the entry point. Force feedback is almost completely lost due to the friction at the air tight trocar and the stiffness of the inflated abdominal wall. There is no tactile sensation at all, which surgeons highly depend on in open surgery to locate arteries and tumors hidden in the tissue.

Minimally invasive surgery itself is telemanipulation as the surgeon is physically separated from the workspace. Therefore, telerobotics is the natural tool to extend capabilities in laparoscopic surgery. With the telesurgical workstation developed, the goal is to replace the manipulation and sensation capabilities of the surgeon which were lost due to minimally invasive surgery. A 6 DOF slave manipulator controlled through a spatially consistent and intuitive master will replace the dexterity, force feedback to the master will give back the fidelity of the manipulation, and tactile feedback will replace lost tactile sensation.

Other work in the literature on telesurgical systems for abdominal surgery include the telesurgical system for open surgery with 4 DOF manipulators developed at SRI International [20] (laparoscopic version is also being developed), the telerobotic assistant for laparoscopic surgery developed by Taylor et.al. [38], and the telesurgery experiments performed between JPL, California and Polytechnic University of Milan, Italy [32], and between Nagoya and Tokyo in Japan [3].

There are other successful medical applications of robotics including systems for orthopedic surgery [39], micro-surgery and stereotactic neurosurgery [23], eye surgery [37], and radiotherapy [42].

This report has two parts. The first part will introduce the UC Berkeley telesurgical workstation, make its kinematic analysis, give information about control issues and describe the implemented control algorithm. In the second part, conceptual and future issues on telesurgery will be presented. First teleoperation issues will be discussed followed by discussions on hybrid control and visualization issues.

Part I

Berkeley/UCSF Telesurgical Workstation

Chapter 2

Description of the System

The Berkeley/UCSF Telesurgical Workstation is a master-slave teleoperation system with two 6 DOF robotic manipulators. The slave manipulator is composed of two parts. The first part is the gross positioning stage which is located outside the body. It is responsible for positioning the millirobot, which is the second part. The gross stage controls the same 4 DOF as those available in conventional laparoscopic instruments. It has a parallel structure, where three linear joints hold a small platform that carries the tool arm and the motor rotating it. All four actuators of this part are DC servo motors. The linear joints are actuated by leadscrews connected to the electric motors. (See figure 2.1)

The millirobot has a 2 DOF wrist located inside the body, and a gripper. It is 10 mm in diameter. Wrist to gripper length is 10 cm, and the tool arm is 24 cm up to the wrist. The millirobot is actuated by hydraulic actuators. Each joint is actuated by a pair of bladders which are inflated with water. The water section is separated from the rest of the hydraulic circuit, utilizing hydraulic fluid, via a set of manifolds. The millirobot is designed to be disposable, and to avoid problems in case of leaks in hydraulics, the bladders will be driven by sterile saline solution.

Performance goals in the design of the millirobot are given in table 2.1. These values are estimated for a suturing task, force and movement requirements for driving a needle through tissue and tying a knot. Table 2.2 gives the experimental measurement results with the actual robot, which are well within the design goals. The specifications adopted for the second version of the system are given in table 2.3.¹

The master manipulator is a 6 DOF serial robot. A commercial 4 DOF force

¹Courtesy of Endorobotics Corp.

Parameter	Value
Dimension: overall diameter	10-15 mm max
Dimension: wrist joint to grasper	100 mm max
Force: at the point of needle, for driving the needle through tissue	1.47 N min
Torque: about grasper axis, for driving needle (assumes curved needle, 15 mm from grasper to needle tip)	2.2 N.cm min
Force: gripping, while driving needle	5 N min
Force: knot tightening tension	2.2 N min
Range of motion: gripper jaw opening	2-3 mm min
Range of motion: rotation about grasper axis, to drive plus allowance for inclined work surface	180-270 degrees min
Range of motion: wrist flexion, for driving needle	90 degrees min
Range of motion: wrist pronation	180 degrees min
Bandwidth	5 Hz min

Table 2.1: Performance goals for the millirobot

Parameter	Measured Value	Target Value
Gripping force	15 N	5 N min
Grasper opening width	6 mm	2-3 mm min
Wrist roll torque	8.8 N.cm	2.2 N.cm min
Wrist roll range of motion	285 degrees	180-270 degrees min
Wrist flexion (yaw) torque	30 N.cm	10-15 N.cm
Bandwidth	~6 Hz	5 Hz

Table 2.2: Millirobot test results

Parameter	Target Value
Wrist joint to grasper length	50 mm max
Gripping force	40 N min
Grasper opening width	8 mm min
Grasper speed: full close in	0.5 sec max
Wrist roll torque	100 N.mm min
Wrist roll range of motion	270 degrees min
Wrist roll speed	540 degrees/sec min
Wrist flexion (yaw) torque	300 N.mm min
Wrist flexion range of motion	90 degrees min
Wrist flexion speed	360 degrees/sec min
Life time	6 months min

Table 2.3: Performance goals for the second version of the millirobot

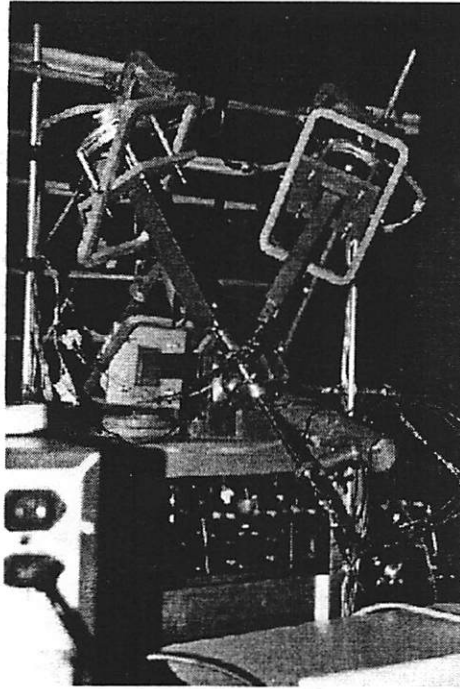


Figure 2.1: Slave manipulator of the Berkeley/UCSF laparoscopic workstation

reflecting joystick (Immersion Impulse Engine 3000) with 3 actuated axes is equipped with an additional 2 DOF (one actuated) and a stylus handle. There are position measurements in all 6 joints and the 4 actuated joints give force feedback in translational directions and the roll axis, where the force is important while driving a needle through tissue. (See figures 2.2 and 2.3).

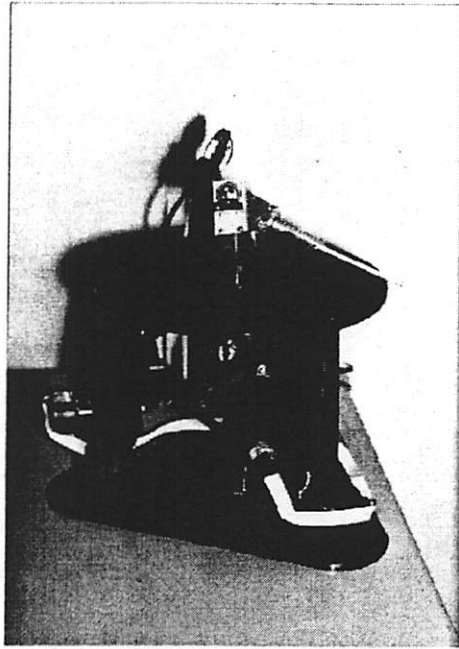


Figure 2.2: Master manipulator of the Berkeley/UCSF laparoscopic workstation

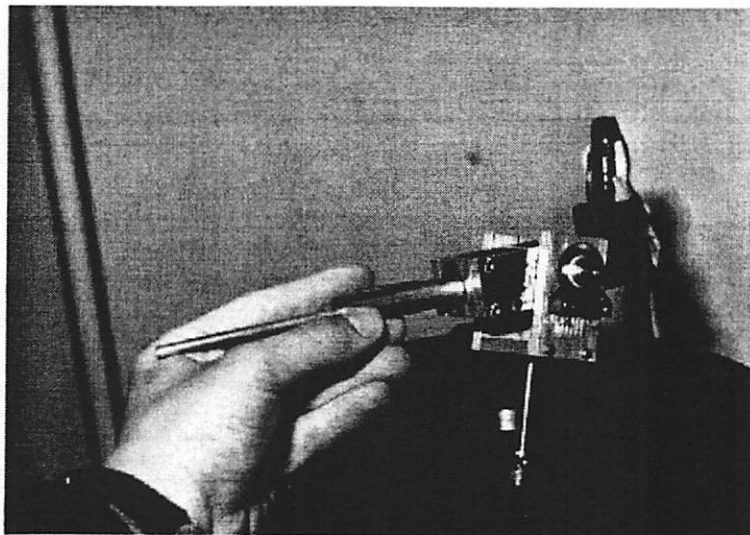


Figure 2.3: Close-up view of the master manipulator

Chapter 3

Kinematics

The master and slave manipulator structures were described in chapter 2. For the control of the system, inverse kinematics of the slave manipulator and forward kinematics of the master manipulator are needed. In this chapter, the explicit solutions of these problems will be derived.

For the kinematic analysis, the product of exponentials formulation is used. Refer to [29] for a full treatment of this formulation.

3.1 Slave Manipulator Inverse Kinematics

To simplify the inverse kinematics calculations, slave kinematics can be divided into two parts: the serial portion inside the body and parallel portion outside the body. The serial part is composed of the fulcrum, which is modeled with a spherical joint and a translational joint, and the 2 DOF wrist. The parallel part of the slave consists of the three arms holding the base of the tool arm, and the tool arm itself. (See figure 3.1)

In the inverse kinematics calculations, first the serial part will be solved, which will give the angles of the wrist joints and the desired configuration of the parallel part. Then the parallel part will be solved to calculate the lengths of the linear joints and the tool arm rotation.

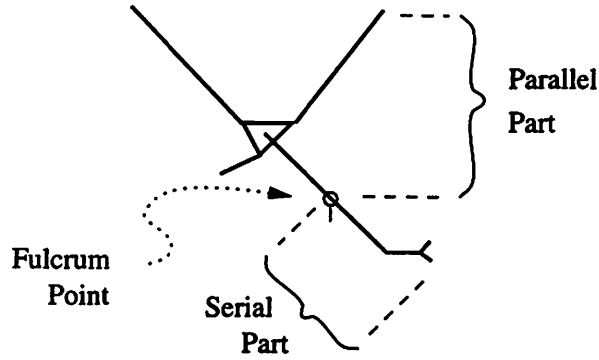


Figure 3.1: Parallel and serial parts of the slave robot

3.1.1 Serial Part

Using the naming convention and the zero configuration shown in figure 3.2, the kinematic configuration of the serial part is characterized by the following twists $\in se(3)$:

$$\xi_{s1} = \begin{bmatrix} 0 \\ 0 \\ 0 \\ 0 \\ 0 \\ 1 \end{bmatrix}, \xi_{s2} = \begin{bmatrix} 0 \\ 0 \\ 0 \\ 0 \\ 1 \\ 0 \end{bmatrix}, \xi_{s3} = \begin{bmatrix} 0 \\ 0 \\ 0 \\ 1 \\ 0 \\ 0 \end{bmatrix}, \xi_{s4} = \begin{bmatrix} 0 \\ 0 \\ 1 \\ 0 \\ 0 \\ 0 \end{bmatrix}, \xi_{s5} = \begin{bmatrix} 0 \\ 0 \\ 0 \\ 0 \\ 1 \\ 0 \end{bmatrix}, \xi_{s6} = \begin{bmatrix} 0 \\ 0 \\ 0 \\ 0 \\ 0 \\ 1 \end{bmatrix} \quad (3.1)$$

and the reference configuration:

$$g_s(0) = \begin{bmatrix} & & & 0 \\ & I_{3 \times 3} & & 0 \\ & & & 0 \\ 0 & 0 & 0 & 1 \end{bmatrix} \in SE(3) \quad (3.2)$$

which gives the forward kinematics map as:

$$g_s(\theta_s) = e^{\hat{\xi}_{s1}\theta_{s1}} e^{\hat{\xi}_{s2}\theta_{s2}} e^{\hat{\xi}_{s3}\theta_{s3}} e^{\hat{\xi}_{s4}\theta_{s4}} e^{\hat{\xi}_{s5}\theta_{s5}} e^{\hat{\xi}_{s6}\theta_{s6}} g_s(0) \quad (3.3)$$

The inverse kinematics of the serial part is straightforward as it is a kinematically simple configuration. Given the desired configuration

$$g_d = \begin{bmatrix} R_d & p_d \\ 0 & 0 & 0 & 1 \end{bmatrix} \in SE(3) \quad (3.4)$$

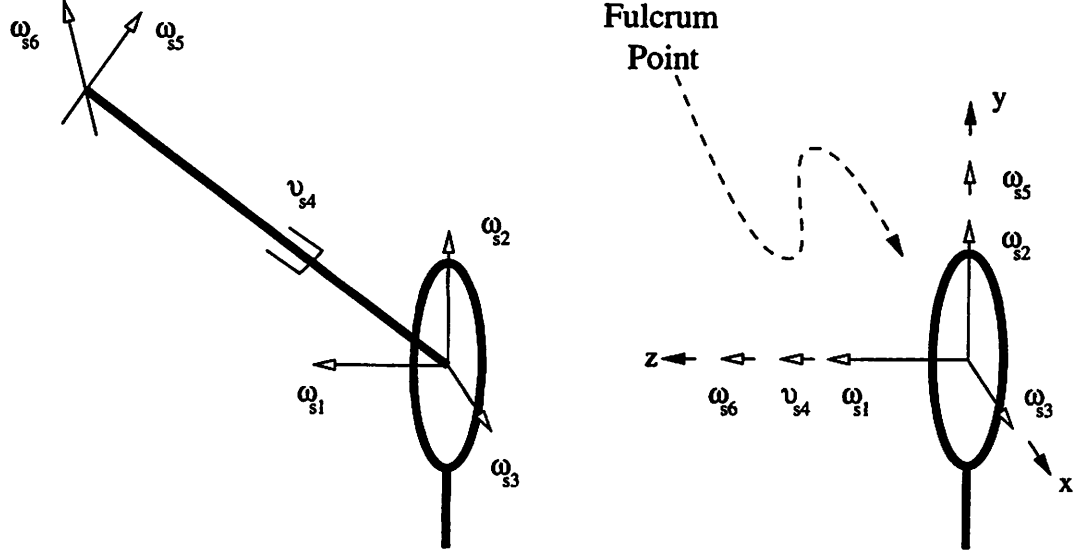


Figure 3.2: Naming convention and the zero configuration of the serial part

θ_{s4} is calculated as:

$$\theta_{s4} = \|p_d\| \quad (3.5)$$

Also observing that the origin $[0 \ 0 \ 0 \ 1]^T$ is invariant under $e^{-\hat{\xi}_{s3}\theta_{s3}} e^{-\hat{\xi}_{s2}\theta_{s2}} e^{-\hat{\xi}_{s1}\theta_{s1}}$:

$$g_s^{-1}(\theta) \begin{bmatrix} 0 \\ 0 \\ 0 \\ 1 \end{bmatrix} = \begin{bmatrix} \theta_{s4} \sin(\theta_{s5}) \cos(\theta_{s6}) \\ -\theta_{s4} \sin(\theta_{s5}) \sin(\theta_{s6}) \\ -\theta_{s4} \cos(\theta_{s5}) \\ 1 \end{bmatrix} \quad (3.6)$$

θ_{s5} and θ_{s6} can be solved as

$$\theta_{s6} = \text{atan2}(-\beta_y, \beta_x) \quad (3.7)$$

and

$$\theta_{s5} = \text{atan2}(\mp \sqrt{\beta_x^2 + \beta_y^2}, -\beta_z) \quad (3.8)$$

where

$$\beta = g_d^{-1} \begin{bmatrix} 0 \\ 0 \\ 0 \\ 1 \end{bmatrix} \quad (3.9)$$

Here, note that θ_{s5} has two solutions, and θ_{s6} can have any value when $\theta_{s5} = 0$, which is a singular configuration. Then,

$$e^{\hat{\xi}_{s1}\theta_{s1}} e^{\hat{\xi}_{s2}\theta_{s2}} e^{\hat{\xi}_{s3}\theta_{s3}} = g_d e^{-\hat{\xi}_{s6}\theta_{s6}} e^{-\hat{\xi}_{s5}\theta_{s5}} e^{-\hat{\xi}_{s4}\theta_{s4}} \quad (3.10)$$

which will be used in the solution of the parallel part, since ξ_{s1} , ξ_{s2} , and ξ_{s3} form the fictitious ball joint at the entry point.

3.1.2 Parallel Part

The parallel part of the platform consists of three arms, connected to a triangular base which holds the millirobot. Two of the arms have 6 DOF, whereas the third one has only five. In all of the arms, only 1 DOF, the translational joint, is actuated. The solution of the inverse kinematics for the parallel part requires finding the lengths of these translational joints and calculating the rotation of the tool arm. We will first proceed to solve the inverse kinematics of the 5 DOF arm, then use this to calculate the lengths of the prismatic joints in the other two arms, and the rotation.

Specification of the Configuration

Figure 3.3 gives a side view of the parallel part, showing the joint naming conventions and various point and coordinate frames used in the calculations. In the figure, joints 1–5 are on the 5 DOF arm, and joint 6 is the rotation of the tool arm. The serial part of the inverse kinematics gives the direction \hat{n}_f , which is determined from the spherical joint at the fulcrum, as:

$$\hat{n}_f = e^{\hat{\xi}_{s1}\theta_{s1}} e^{\hat{\xi}_{s2}\theta_{s2}} e^{\hat{\xi}_{s3}\theta_{s3}} \begin{bmatrix} 0 \\ 0 \\ 1 \\ 0 \end{bmatrix} \quad (3.11)$$

and the length d :

$$d = \theta_{s4} \quad (3.12)$$

As notation, the subscripts of points and vectors denote the coordinate frames in which they are expressed. The subscripts of the homogeneous transforms denote which coordinate frames they transform. Also, $\langle \cdot, \cdot \rangle$ is used to denote inner product.

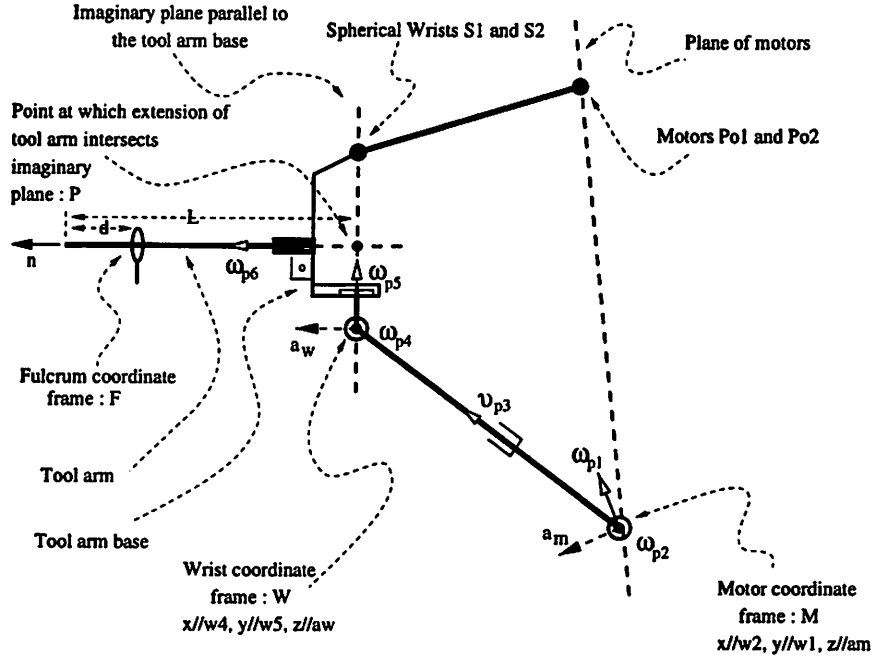


Figure 3.3: Kinematic diagram of the side view of parallel section

The forward kinematics of the 5 DOF arm, choosing the zero configuration as W overlapped with M , are:

$$g_{mw}(\theta_p) = e^{\xi_{p1}\theta_{p1}} e^{\xi_{p2}\theta_{p2}} e^{\xi_{p3}\theta_{p3}} e^{\xi_{p4}\theta_{p4}} e^{\xi_{p5}\theta_{p5}} g_{mw}(0) \quad (3.13)$$

where,

$$\xi_{p1} = \begin{bmatrix} 0 \\ 0 \\ 0 \\ 0 \\ 1 \\ 0 \end{bmatrix}, \xi_{p2} = \begin{bmatrix} 0 \\ 0 \\ 0 \\ 1 \\ 0 \\ 0 \end{bmatrix}, \xi_{p3} = \begin{bmatrix} 0 \\ 0 \\ 1 \\ 0 \\ 0 \\ 0 \end{bmatrix}, \xi_{p4} = \begin{bmatrix} 0 \\ 0 \\ 0 \\ 1 \\ 0 \\ 0 \end{bmatrix}, \xi_{p5} = \begin{bmatrix} 0 \\ 0 \\ 0 \\ 0 \\ 1 \\ 0 \end{bmatrix}, g_{mw}(0) = I_{4 \times 4} \quad (3.14)$$

The homogeneous transform between the M and F coordinate frames (g_{mf}), W coordinates of the spherical wrists S_1 and S_2 , and M coordinates of the centers of the other two motors P_{o1} and P_{o2} are all known as they are constant.

The point at which extension of the tool arm intersects the (imaginary) plane passing through the wrists on the tool base is defined as P . Note that P has W coordinates

of the form:

$$p_w = \begin{bmatrix} 0 & p_{wy} & 0 & 1 \end{bmatrix}^T \quad (3.15)$$

and equations 3.11 and 3.12 give

$$p_f = -(L - d)\hat{n}_f + \begin{bmatrix} 0 \\ 0 \\ 0 \\ 1 \end{bmatrix} \quad (3.16)$$

where L is the length of the tool arm.

Solution of the Inverse Kinematics

First, the unknowns $\theta_{p1} \dots \theta_{p5}$ are solved using the following equations:

- The z axis of W points in the same direction as \hat{n} :

$$g_{mw} \begin{bmatrix} 0 \\ 0 \\ 1 \\ 0 \end{bmatrix} = g_{mf} \hat{n}_f \quad (3.17)$$

$$\begin{bmatrix} \sin(\theta_{p1}) \cos(\theta_{p2} + \theta_{p4}) \cos(\theta_{p5}) + \cos(\theta_{p1}) \sin(\theta_{p5}) \\ -\cos(\theta_{p5}) \sin(\theta_{p2} + \theta_{p4}) \\ \cos(\theta_{p1}) \cos(\theta_{p2} + \theta_{p4}) \cos(\theta_{p5}) - \sin(\theta_{p1}) \sin(\theta_{p5}) \\ 0 \end{bmatrix} = \hat{n}_m \quad (3.18)$$

- The origin of W and the point P lie on the imaginary plane passing through the wrists on the base, which is perpendicular to \hat{n} :

$$\left\langle g_{mw} \begin{bmatrix} 0 \\ 0 \\ 0 \\ 1 \end{bmatrix}, g_{mf} \hat{n}_f \right\rangle = \left\langle g_{mf} p_f, g_{mf} \hat{n}_f \right\rangle \quad (3.19)$$

$$\theta_{p3}(n_{mz} \cos(\theta_{p1}) \cos(\theta_{p2}) + n_{mx} \cos(\theta_{p2}) \sin(\theta_{p1}) - n_{my} \sin(\theta_{p2})) = \langle p_m, \hat{n}_m \rangle \quad (3.20)$$

- The transform of p_w through g_{mw} is the same as transform of p_f through g_{mf} , as they are coordinates of the same point, P :

$$g_{mw}p_w = g_{mf}p_f \quad (3.21)$$

$$\begin{bmatrix} \sin(\theta_{p1})(\theta_{p3} \cos(\theta_{p2}) + p_{wy} \sin(\theta_{p2} + \theta_{p4})) \\ p_{wy} \cos(\theta_{p2} + \theta_{p4}) - \theta_{p3} \sin(\theta_{p2}) \\ \cos(\theta_{p1})(\theta_{p3} \cos(\theta_{p2}) + p_{wy} \sin(\theta_{p2} + \theta_{p4})) \\ 1 \end{bmatrix} = p_m \quad (3.22)$$

Note that although there are 7 equations (3.18,3.20, and 3.22) in 5 unknowns, some of them are dependent. That is why these equations can be solved.

θ_{p1} can be immediately solved from the first and third rows of the equation (3.22):

$$\theta_{p1} = \text{atan2}(p_{mx}, p_{mz}) \quad (3.23)$$

Note that the term multiplying $\sin(\theta_{p1})$ and $\cos(\theta_{p1})$ is always positive in the physically possible workspace of the manipulator.

Then, eliminating $\sin(\theta_{p5})$ from first and third rows of equation (3.18) and solving for $\cos(\theta_{p2} + \theta_{p4}) \cos(\theta_{p5})$:

$$\cos(\theta_{p2} + \theta_{p4}) \cos(\theta_{p5}) = n_{mz} \cos(\theta_{p1}) + n_{mx} \sin(\theta_{p1}) \quad (3.24)$$

Then, $\theta_{p2} + \theta_{p4}$ can be solved using the second row of equation (3.18) and equation (3.24):

$$\theta_{p2} + \theta_{p4} = \text{atan2}(-n_{my}, n_{mz} \cos(\theta_{p1}) + n_{mx} \sin(\theta_{p1})) \quad (3.25)$$

Here, note that $\cos(\theta_{p5})$ cannot be zero practically.

Assuming $\theta_{p3} \neq 0$, which is also practically true, first $\theta_{p3} \cos(\theta_{p2})$ can be solved from third row of equation (3.22):

$$\theta_{p3} \cos(\theta_{p2}) = \frac{p_{mz}}{\cos(\theta_{p1})} - p_{wy} \sin(\theta_{p2} + \theta_{p4}) \quad (3.26)$$

and then used to calculate θ_{p2} using the second row of equation (3.22):

$$\theta_{p2} = \text{atan2}(p_{wy} \cos(\theta_{p2} + \theta_{p4}) - p_{my}, \frac{p_{mz}}{\cos(\theta_{p1})} - p_{wy} \sin(\theta_{p2} + \theta_{p4})) \quad (3.27)$$

If $\cos(\theta_{p1}) \approx 0$, to avoid division by zero, $\theta_{p3} \cos(\theta_{p2})$ can be solved from row 1 of equation (3.22):

$$\theta_{p3} \cos(\theta_{p2}) = \frac{p_{mx}}{\sin(\theta_{p1})} - p_{wy} \sin(\theta_{p2} + \theta_{p4}) \quad (3.28)$$

giving

$$\theta_{p2} = \text{atan2}(p_{wy} \cos(\theta_{p2} + \theta_{p4}) - p_{my}, \frac{p_{mx}}{\sin(\theta_{p1})} - p_{wy} \sin(\theta_{p2} + \theta_{p4})) \quad (3.29)$$

Then, θ_{p3} can be calculated from equation (3.20):

$$\theta_{p3} = \frac{\langle p_m, \hat{n}_m \rangle}{n_{mx} \cos(\theta_{p1}) \cos(\theta_{p2}) + n_{mx} \cos(\theta_{p2}) \sin(\theta_{p1}) - n_{my} \sin(\theta_{p2})} \quad (3.30)$$

Here, note that as θ_{p3} and the right hand side of equation 3.20 cannot be zero, there will not be division by zero.

Then θ_{p5} can be solved from the first row of (3.18), by first replacing $\cos(\theta_{p2} + \theta_{p4}) \cos(\theta_{p5})$ calculated earlier. A little manipulation, using the facts that $\cos(\theta_{p1}) \neq 0$ practically, and $\theta_{p5} \in (-\pi/2, \pi/2)$, yields:

$$\theta_{p5} = \arcsin(n_{mx} \cos(\theta_{p1}) - n_{mz} \sin(\theta_{p1})) \quad (3.31)$$

It is also possible to get a formula in $\text{atan2}(\cdot, \cdot)$ for higher precision, using the second row of equation (3.18) or the formula for $\cos(\theta_{p2} + \theta_{p4}) \cos(\theta_{p5})$ derived in equation (3.24) above, depending on the value of $\theta_{p2} + \theta_{p4}$. For $\sin(\theta_{p2} + \theta_{p4}) \neq 0$:

$$\theta_{p5} = \text{atan2}(n_{mx} \cos(\theta_{p1}) - n_{mz} \sin(\theta_{p1}), \frac{-n_{my}}{\sin(\theta_{p2} + \theta_{p4})}) \quad (3.32)$$

and for $\sin(\theta_{p2} + \theta_{p4}) \approx 0$:

$$\theta_{p5} = \text{atan2}(n_{mx} \cos(\theta_{p1}) - n_{mz} \sin(\theta_{p1}), \frac{n_{mz} \cos(\theta_{p1}) + n_{mx} \sin(\theta_{p1})}{\cos(\theta_{p2} + \theta_{p4})}) \quad (3.33)$$

Once p_m and g_{mw} are known, remaining unknowns, the other two lengths and the rotation, can be easily solved:

$$l_1 = \|g_{mw} s_{1w} - p_{o1m}\| \quad (3.34)$$

$$l_2 = \|g_{mw} s_{2w} - p_{o2m}\| \quad (3.35)$$

$$\alpha = g_{mw}^{-1} e^{\hat{e}_{s1}\theta_{s1}} e^{\hat{e}_{s2}\theta_{s2}} e^{\hat{e}_{s3}\theta_{s3}} \begin{bmatrix} 1 \\ 0 \\ 0 \\ 0 \end{bmatrix} \quad (3.36)$$

$$\theta_{p6} = \text{atan2}(\alpha_y, \alpha_x) \quad (3.37)$$

which gives the forward kinematics map as:

$$\begin{aligned}
g_m(\theta_m) &= e^{\hat{\xi}_{m0}\theta_{m0}} e^{\hat{\xi}_{m1}\theta_{m1}} e^{\hat{\xi}_{m2}\theta_{m2}} e^{\hat{\xi}_{m3}\theta_{m3}} e^{\hat{\xi}_{m4}\theta_{m4}} e^{\hat{\xi}_{m5}\theta_{m5}} g_m(0) \quad (3.40) \\
&= \begin{bmatrix}
c_5 (c_0 c_3 + s_0 s_1 s_3) + (-c_1 c_4 s_0) + (-c_3 s_0 s_1) + c_0 s_3 s_4 s_5 \\
\quad - (c_1 c_5 s_3) + (-c_4 s_1) + c_1 c_3 s_4 s_5 \\
c_5 (c_3 s_0 - c_0 s_1 s_3) + (c_0 c_1 c_4 + (c_0 c_3 s_1 + s_0 s_3) s_4) s_5 \\
\quad 0 \\
c_4 (-c_3 s_0 s_1) + c_0 s_3 s_4 + c_1 s_0 s_4 \\
\quad c_1 c_3 c_4 + s_1 s_4 \\
c_4 (c_0 c_3 s_1 + s_0 s_3) - c_0 c_1 s_4 \\
\quad 0 \\
c_5 (-c_1 c_4 s_0) + (-c_3 s_0 s_1) + c_0 s_3 s_4 - (c_0 c_3 + s_0 s_1 s_3) s_5 \\
\quad c_5 (-c_4 s_1) + c_1 c_3 s_4 + c_1 s_3 s_5 \\
c_5 (c_0 c_1 c_4 + (c_0 c_3 s_1 + s_0 s_3) s_4) - (c_3 s_0 - c_0 s_1 s_3) s_5 \\
\quad 0 \\
-(h c_1 s_0) - \theta_2 c_1 s_0 + w c_3 c_4 s_0 s_1 - w c_0 c_4 s_3 - w c_1 s_0 s_4 \\
\quad - (w c_1 c_3 c_4) - h s_1 - \theta_2 s_1 - w s_1 s_4 \\
h c_0 c_1 + \theta_2 c_0 c_1 - w c_0 c_3 c_4 s_1 - w c_4 s_0 s_3 + w c_0 c_1 s_4 \\
\quad 1
\end{bmatrix} \quad (3.41)
\end{aligned}$$

and the body Jacobian of the manipulator as:

$$\begin{bmatrix}
-((h + \theta_2) c_4 c_5 (c_1 c_3 c_4 + s_1 s_4)) - (w + h s_4 + \theta_2 s_4) (-c_4 c_5 s_1) + c_1 (c_3 c_5 s_4 + s_3 s_5) \\
\quad - ((h + \theta_2) c_1 c_4 s_3) \\
(h + \theta_2) c_4 (c_1 c_3 c_4 + s_1 s_4) s_5 - (-w - h s_4 - \theta_2 s_4) (-c_4 s_1 s_5) + c_1 (-c_5 s_3 + c_3 s_4 s_5) \\
\quad c_4 s_1 s_5 - c_1 (-c_5 s_3 + c_3 s_4 s_5) \\
\quad - (c_1 c_3 c_4) - s_1 s_4 \\
\quad c_4 c_5 s_1 - c_1 (c_3 c_5 s_4 + s_3 s_5) \\
(h + \theta_2) c_4^2 c_5 s_3 + (w + h s_4 + \theta_2 s_4) (c_5 s_3 s_4 - c_3 s_5) \\
\quad - ((h + \theta_2) c_3 c_4) \\
-((h + \theta_2) c_4^2 s_3 s_5) + (-w - h s_4 - \theta_2 s_4) (c_3 c_5 + s_3 s_4 s_5) \\
\quad c_3 c_5 + s_3 s_4 s_5 \\
\quad c_4 s_3 \\
\quad c_5 s_3 s_4 - c_3 s_5 \\
c_4 s_5 \quad - (w c_4 c_5) \quad w s_5 \quad 0 \\
-s_4 \quad 0 \quad 0 \quad 0 \\
c_4 c_5 \quad w c_4 s_5 \quad w c_5 \quad 0 \\
0 \quad - (c_4 s_5) \quad -c_5 \quad 0 \\
0 \quad s_4 \quad 0 \quad -1 \\
0 \quad - (c_4 c_5) \quad s_5 \quad 0
\end{bmatrix} \quad (3.42)$$

where c_i and s_i denote $\cos(\theta_{mi})$ and $\sin(\theta_{mi})$ respectively.

Chapter 4

Control

4.1 Open Loop Issues

The main bottleneck in the dynamics of the slave manipulator is the lag in the hydraulic actuators, which is due to the transmission delay in the tubing, and the first order lag resulting from the *RC effect* of the tube-bladder configuration. A simple model for transmission delay in the pipes considering the compressibility of water and elasticity of tubes, but neglecting the viscous effects present, gives the propagation velocity of the pressure wave fronts as [33]:

$$c = \sqrt{\frac{\frac{K}{\rho}}{1 + \frac{Kd}{Et}}} \quad (4.1)$$

where c is the propagation velocity, K is the bulk modulus of water, ρ is the density of water, d is the diameter of the tube, t is the thickness of the tube, and E is the linear modulus of elasticity of the tube material. The tubes connecting the manifolds to the bladders are composed of two sections. Thick section tubes have $d/t = 3.5$ and are made of Nylon 11, with $E = 0.5 \times 10^3 \text{psi}$. Thin section tubes have $d/t = 2.2$ and are made of PTFE, which has $E = 33\text{--}65 \times 10^3 \text{psi}$. Calculations estimate the time delay as 28.6msec in the thick section and $1.3\text{--}1.6 \text{msec}$ in the thin sections, which is very close to the experimentally measured values of $32\text{--}38 \text{msec}$. We are currently working on the model of the whole hydraulic system, including the viscous effects, to optimize the design parameters.

The parallel structure of the gross stage prevents designing a dynamics based control algorithm (like a computed torque algorithm). Backlash in the linear actuators of gross stage is another point to keep in mind for the controller design. The quadratic position

vs. angle characteristics (see figure 4.1) of the Hall effect sensors used for position feedback from millirobot need to be compensated in the controller.

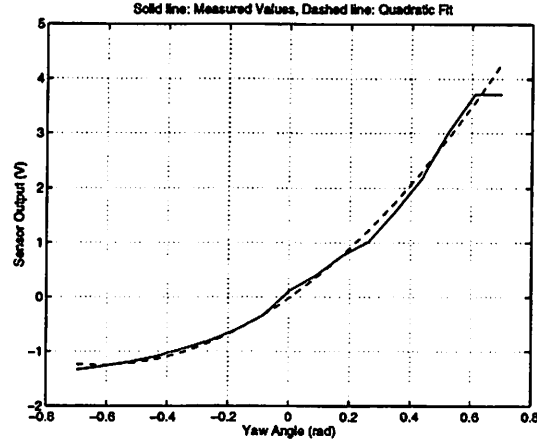


Figure 4.1: Yaw sensor input-output characteristic

4.2 Control Algorithm

The overall structure of the proposed control design for the telesurgical workstation is shown in figure 4.2. In the current implementation, which is shown in figure 4.3, the force and tactile loops and safety monitor are not present. A small dead-band is put at the error signal for linear joints to avoid oscillations due to backlash. Anti-windup integral terms (with saturation) are used in the PID controllers. The sensor outputs are compensated for the nonlinear input-output characteristics.

4.3 Discussion

Bandwidth and the time delay for the hydraulic actuators are the limiting factors for the performance of the millirobot. Although parallel structure of the gross stage prevents the use of dynamics based controllers, the high bandwidth actuators used compensate for this.

The safety features not implemented in this prototype controller will be included in the later designs. The independent high level controller, which should run on a separate computer and have an independent set of sensors, is necessary for safety monitoring. The

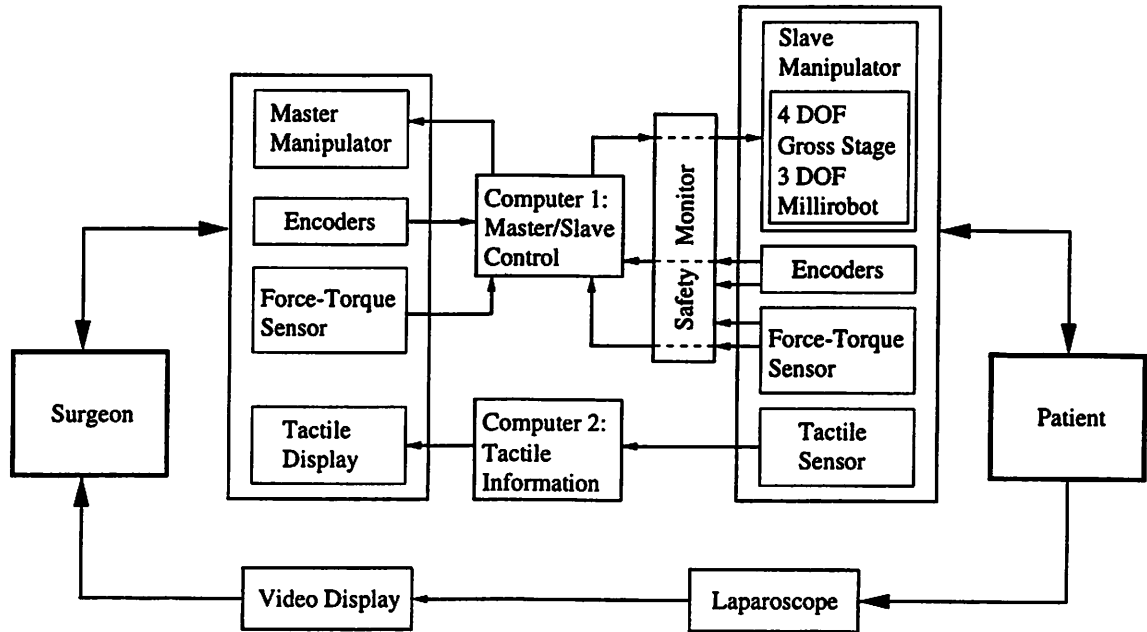


Figure 4.2: Control system block diagram

mission of this safety controller is to monitor the overall system and override commands that violate the safety constraints and to shut down the system in case of failure. A possible low level control algorithm is discussed in chapter 6 to avoid high interaction forces between the manipulator and the surrounding. Increased safety must also be included in the hardware design to compensate for the potential problems in the actuator and sensor systems.

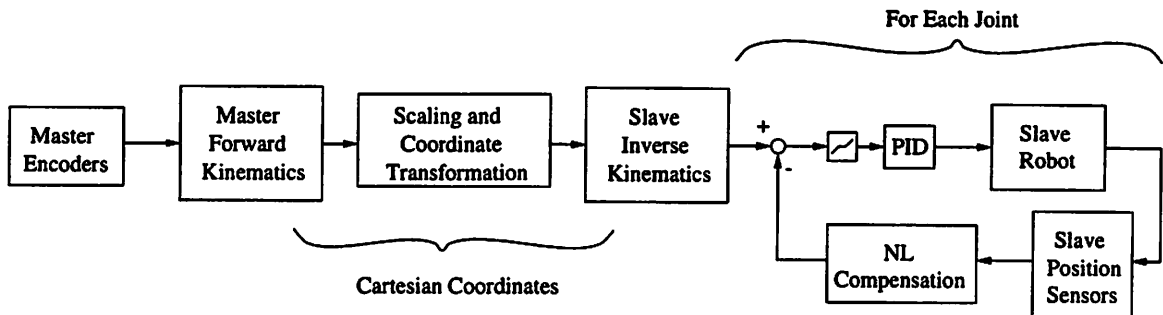


Figure 4.3: Current implementation of master-slave control

Part II

Conceptual and Future Issues in Telesurgery

Chapter 5

Teleoperation for Telesurgery

In this chapter, first, the basic issues of teleoperation will be discussed, and then the control algorithms commonly used in the literature will be introduced in a comparative manner. Throughout the discussion, special emphasis will be given on issues critical to the application at hand — telesurgery. More general treatments of teleoperation can be found in [35, 36, 6].

The main concerns for telesurgery can be summarized as follows:

- Need for force-torque feedback
- Stability under time delay
- Fidelity and performance

which will affect the choice of control algorithm and hardware for sensing and computation.

5.1 Basic Issues — Stability-Fidelity Trade-off

The master-slave teleoperation system can be represented with the simple block diagram of figure 5.1.

There is not a single agreed formulation for the ideal response for master-slave teleoperation systems. For our purposes we will define the ideal response as perfect position and force tracking of the master and slave manipulators, i.e.

$$x_m(t) \equiv -x_s(t)^1 \tag{5.1}$$

$$f_m(t) \equiv f_s(t) \tag{5.2}$$

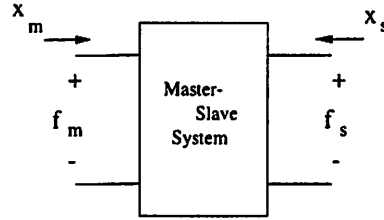


Figure 5.1: Master-slave system representation

This physically corresponds to a massless, infinitely stiff rod connecting the master and slave. Note that this response requires infinite bandwidth and zero time delay, which are not possible practically. So in the practical case, this ideal response can be relaxed to a desired impedance behavior connecting the two manipulators [47], preferably with exponential convergence.

5.1.1 Analysis with Network Equivalents and Two-Port Models

Using a linearity assumption, network equivalents and two-port models can be used for basic analysis of teleoperation systems [17, 18, 31]. These analyses reveal very important qualitative behaviors of master-slave systems. A 1 DOF manipulator model is used in this section as the basis of analysis, but the ideas can be extended to higher DOF.

The network equivalents used are based on the Force-Voltage-Effort and Velocity-Current-Flow analogies between mechanical and electrical systems. This equivalent representation allows the use of compact representations of electrical systems and simulation of systems with easy to use circuit simulators.

In this analogy:

Effort: Force f analogous to voltage V

Flow: Velocity v analogous to current I

$$f = bv \sim V = RI \quad (5.3)$$

$$f = k \int v dt \sim V = \frac{1}{C} \int I dt \quad (5.4)$$

$$v = \frac{1}{m} \int f dt \sim I = \frac{1}{L} \int V dt \quad (5.5)$$

The components are like impedances. Flow and effort sources are defined in the usual way.

¹Note that directions of x_m and x_s are defined reverse. See figure 5.1.

The master-slave teleoperation system model we have presented above (linear or non-linear) can be represented as a two-port network. The ports are the handles of the master and the slave end-effector.

With a *linearity* assumption, this two-port network can be represented with a 2×2 matrix. As it is possible to represent the ideal/desired response in terms of the two-port parameters, this representation provides a framework for the analysis of the effects of system components on the overall response.

The discussion here will be based on hybrid parameters of a two-port network, following [17]. However the results are general, and can be deduced from other parameters as well.

The hybrid parameters of a two-port network is defined as:

$$\begin{bmatrix} e_{in} \\ i_{out} \end{bmatrix} = \begin{bmatrix} h_{11} & h_{12} \\ h_{21} & h_{22} \end{bmatrix} \begin{bmatrix} i_{in} \\ e_{out} \end{bmatrix} \quad (5.6)$$

where e stands for effort variable and i stands for flow variable, with

$$\begin{aligned} h_{11} &= \left. \frac{e_{in}}{i_{in}} \right|_{e_{out}=0}, & h_{12} &= \left. \frac{e_{in}}{e_{out}} \right|_{i_{in}=0} \\ h_{21} &= \left. \frac{i_{out}}{i_{in}} \right|_{e_{out}=0}, & h_{22} &= \left. \frac{i_{out}}{e_{out}} \right|_{i_{in}=0} \end{aligned} \quad (5.7)$$

Then the ideal response we have defined above can be expressed in terms of these h-parameters as:

$$H = \begin{bmatrix} 0 & \text{Reverse Force Scale} \\ \text{Velocity Scale} & 0 \end{bmatrix} = \begin{bmatrix} 0 & 1 \\ -1 & 0 \end{bmatrix} \quad (5.8)$$

The bilateral master-slave teleoperation system, together with the environment and the human operator, forms a closed loop control system (see figure 5.2). In order to make a stability analysis, it is necessary to calculate the open loop transfer function. The forward path is from the command of the human operator, τ_{op} , to the output, slave manipulator velocity, and the return path is from the interaction force at the slave end-effector sent back to human operator. Then the open loop transfer function is $G_{loop} = G_1 G_2$, where forward path transfer function is $G_1(s)$ and reverse path transfer function is $G_2(s)$. Time delay will also be introduced in this analysis, as it is critical for the stability. The loop (2-way) delay is denoted with T .

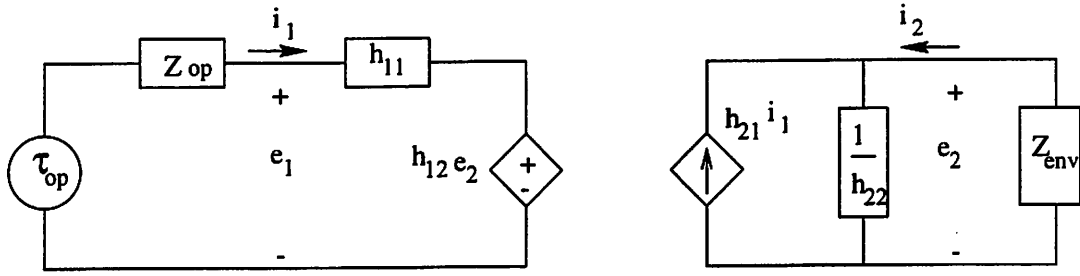


Figure 5.2: Master-slave system coupled with operator and environment

Calculations yield

$$G_{loop} = G_1 G_2 = e^{-sT} \frac{h_{12} h_{21} Z_{env}}{(h_{11} + Z_{op})(1 + h_{22} Z_{env})} \quad (5.9)$$

as the loop gain. (Refer to [18] for details of calculation)

For the “ideal” case, with $h_{11} = 0$, $h_{12} = 1$, $h_{21} = -1$, $h_{22} = 0$, the loop gain will be:

$$G_{loop} = -e^{-sT} \frac{Z_{env}}{Z_{op}} \quad (5.10)$$

Then, for hard contact, where $Z_{env} \gg Z_{op}$, the system goes unstable very easily, i.e. the operation bandwidth must be severely limited.

From this, the worst case scenario can be identified as when the human operator releases the handle ($Z_{op} \rightarrow 0$) and the slave makes a hard contact ($Z_{env} \rightarrow \infty$). Then,

$$G_{loop} = e^{-sT} \frac{h_{21} h_{12} Z_s}{Z_m} \quad (5.11)$$

$$= e^{-sT} \frac{h_{21} h_{12}}{h_{11} h_{22}} \quad (5.12)$$

Here, the tradeoff between stability and fidelity can be clearly seen. For stability, it is desirable to have $|h_{11} h_{22}|$ as large as possible, whereas for fidelity, it is desirable for $|h_{11} h_{22}|$ to be close to 0.

5.2 Control Algorithms Overview

This section aims to give an overview of the various control algorithms for teleoperation present in the literature, and to compare them in the context of our application.

The challenges of telesurgery are quite different from conventional teleoperation applications. As we are manipulating soft tissue, stability is less of a problem, whereas, there is a significant need for fidelity during telemanipulation.

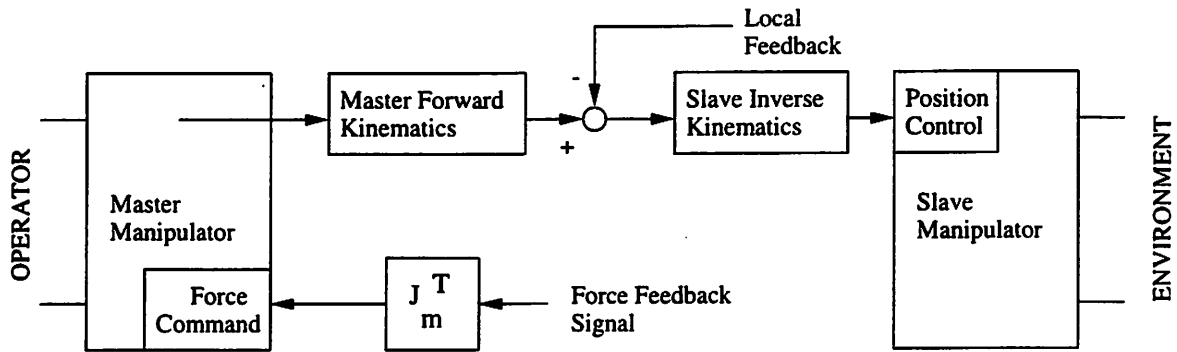


Figure 5.3: Block diagram of a typical 6 DOF position control based algorithm

As shown in the previous section, there has to be a compromise between stability and fidelity of teleoperation algorithms. The control algorithms available in literature can be classified in terms of this trade-off [25]. For example, the passive communication based control algorithms of [30, 1, 2] are optimized for stability and have poor fidelity [24], whereas the control algorithms of [47, 48] for ideal kinesthetic coupling are optimized for fidelity and have poor stability.

In section 5.2.1 implementations of some selected algorithms from literature will be briefly summarized.

Experimental comparisons of the position control based (with various kind of force feedback) and passive communication based control algorithms in conventional teleoperation tasks will be summarized in section 5.2.2 from [11, 22, 19, 24].

In section 5.3, applicability of various algorithms to our application will be discussed.

5.2.1 Control Algorithms

Position Control Based Algorithms

The generic block diagram of this class of control algorithms is given in figure 5.3. Slave side is under a position control law, such as PD control, tracking the position of master. Examples of this class of controllers can be found in [11, 17, 4].

There are three main variations in this type of control. First is the addition of remote site compliance (RSC). The idea here is to alter the position command received from the master depending on the interaction force. This results in increased compliance

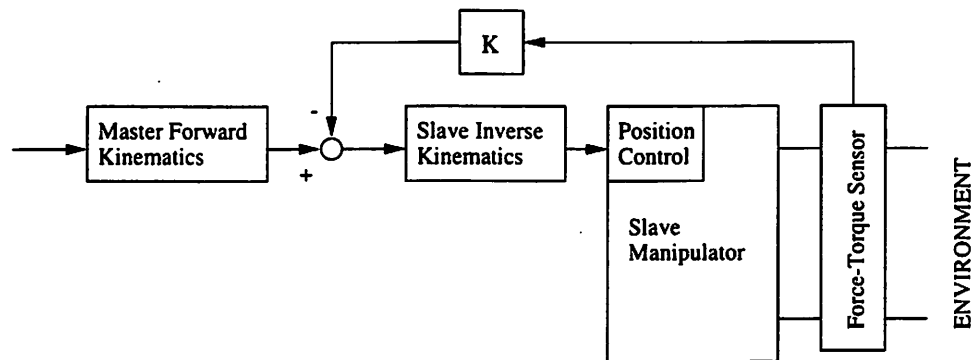


Figure 5.4: Remote site compliance

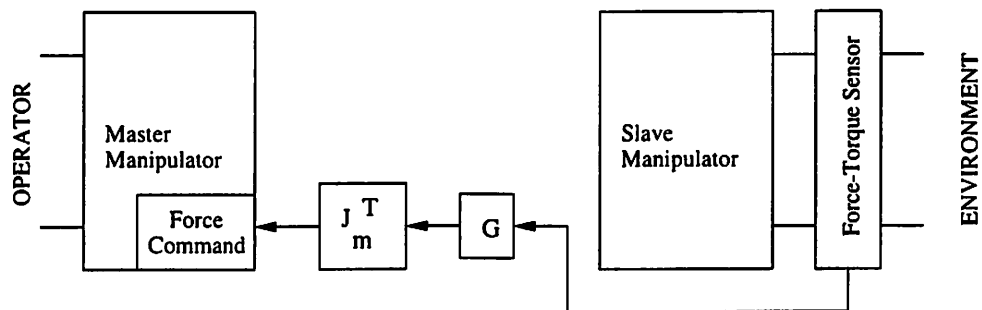


Figure 5.5: Kinesthetic force feedback

and has a stabilizing effect (see [18]). The general form of this approach is in figure 5.4.

The other variations are based on the type of force feedback to the master. In kinesthetic force feedback (KFF), the interaction force between the slave and environment is measured with a force-torque sensor and used as the feedback signal to master. The general form is shown in figure 5.5. In position-error based force feedback (PEFF), the error between the master and slave positions is used as the feedback signal to master. Its general form is given in figure 5.6. Force feedback in teleoperation increases the performance but has stability problems under time delay (especially KFF).

Passive Communication Based Control Algorithms

A simple analysis reveals that the time delay in communication channel results in the loss of passivity of the communication channel. In passive communication based control algorithms, the idea is to use an analogy to wave propagation in transmission lines to guarantee the passivity of the communication channel under arbitrary time delay. The

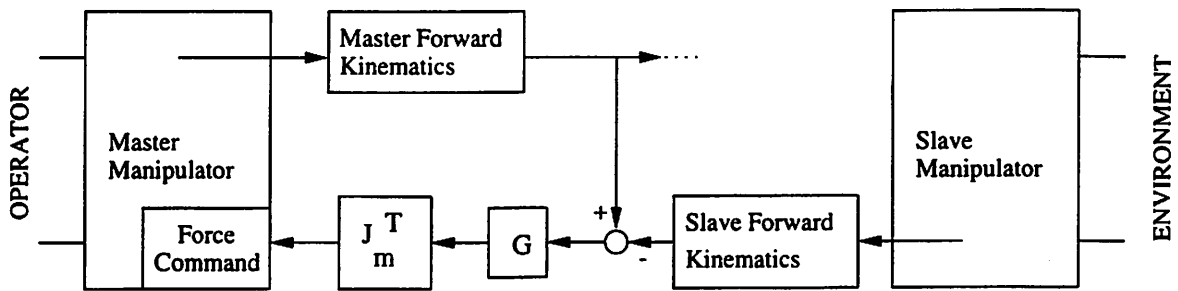


Figure 5.6: Position error based force feedback

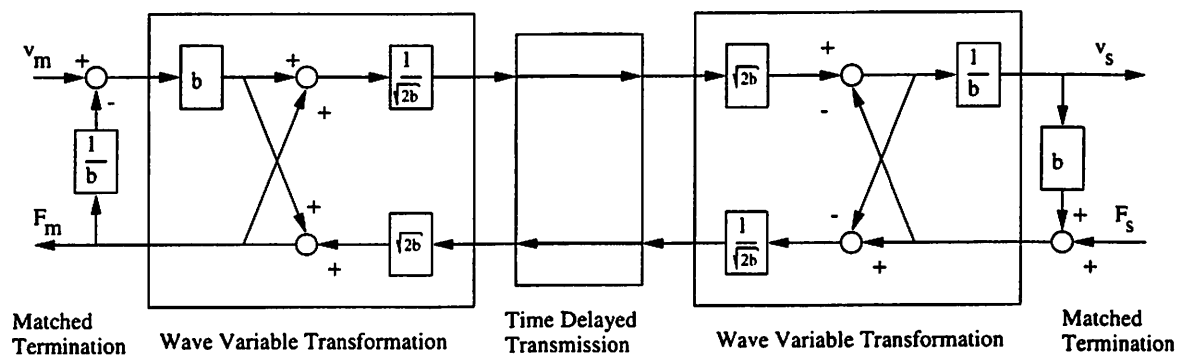


Figure 5.7: Block diagram of a passive communication block

resulting passive communication block has the general form given in figure 5.7. Details of this approach can be found at [30, 1, 2]. With this control, the stability of the overall system can be guaranteed, but the drawback is reduced effective stiffness of the manipulator.

Control for Ideal Kinesthetic Coupling

In this approach, the idea is to achieve perfect position and force tracking between the master and slave manipulators. With this definition of ideal response, the master-slave system behaves like an infinitely stiff massless rod. This type of control is model based, and requires measurement and transmission of position, velocity, acceleration and force in both directions [48].

This control algorithm is sensitive to model uncertainties which results in stability problems. Therefore, a practical variation of this algorithm, in which the master-slave system behaves like a specified impedance rather than a massless infinitely stiff rod, is more applicable. The introduced impedance has a stabilizing effect. It is also possible to achieve

low frequency transparency without acceleration transmission [25].

Other Approaches

There are also some other control approaches in literature, such as H-infinity control [46], virtual internal model following control [14], impedance shaping control [10] etc., which may be applicable to telesurgery. However, there are either not enough experimental results to compare them or they are not fundamentally different in nature.

Rate control (maybe with various types of feedback), is another class of control where the position of the master device controls the velocity of the slave rather than position. It has specific applications, but it is not suitable for telesurgery at all because of its non-intuitive nature, and therefore not explained in this report. Information and experimental comparisons on them can be found in [11].

5.2.2 Experimental Comparison of Algorithms in Conventional Teleoperation Tasks

Results discussed in this section are summarized from [11, 22, 19, 24].

In the literature, the following criteria are used in comparing various algorithms:

- Task Completion Time
- Peak Force
- Sum of Squared Forces
- Number of Errors
- Post-Experiment Survey on the Qualitative Feel of the System

Another criterion, which has not been used, but is of significant importance, is the learning curves for some of the above measures.

The tasks used in [11, 22, 19] are usually peg-in-hole and pick-and-place *type* of tasks in a satellite repair setting with a 6 DOF manipulator with simulated time delays up to 4 sec. A constant force maintaining task is also used. In [24] the tasks used were 1 DOF constant force maintaining, and pointing (simple pointing and pointing under the influence of a non-linear stiffness) tasks. The experiment conditions included simulated communication delays up to 1 sec.

As the result of the studies [11, 22, 19] comparing the position control based algorithms (with no feedback, KFF, RSC, KFF+RSC, PEFF, PEFF+RSC) the authors recommend the use of KFF+RSC for short time delay (up to 0.5-1 sec.) and just RSC for longer time delays. They note that force feedback increases the performance, but causes instability problems under time delay; whereas, remote site compliance has a stabilizing effect as well as reducing the interaction forces. They also propose the use of task level parameter selection, i.e. selection of compliance parameters depending on the task to be performed. For no time delay operation, they favor KFF and shared modes.

In [24], Lawn and Hannaford compare position control based (with no feedback, KFF) and passive communication based control algorithms. They conclude that passive communication based control algorithm has poor performance at the given tasks (50% longer completion time compared to the other algorithms, even at no time delay) due to reduces stiffness, and the performance degrades severely fast with increasing time delay. (They also note that KFF algorithm starts to have instability problems at time delays as low as 60ms.)

5.3 Discussion in the Context of Telesurgery

Force feedback is important for telesurgery because of high level of interaction with the environment. Although currently there are not any direct experimental results, the performance increase as a result of force feedback in conventional teleoperation tasks is a clear indication as interaction in telesurgery is more critical and delicate.

The limiting factor for telesurgery will be the fidelity of teleoperation, especially under time delay. Although the control algorithms stabilized via RSC are reported to perform reasonably well for conventional teleoperation tasks, they are not satisfactory enough for surgery because of the lost fidelity as a result of the reduced stiffness of the manipulator. As the telesurgical workstation manipulator itself is not very stiff, and it will be manipulating soft tissue, RSC would not be necessary for stability (at least for short time delay).

For increased fidelity, performance of model based controllers will be needed, at the expense of increased computational burden. Especially, model based control (or at least gravity compensation) on the master side is critical for better fidelity and to avoid fatigue. Increased force fidelity of a force sensor on the slave, compared to position error based force

feedback might be desirable.

In telesurgery, small positional errors (including the no time delay case) can be tolerated as the robot will be moving under visual guidance of surgeon.

For operation under short time delay, the compliance of robot and environment would be enough for stable operation with kinesthetic force feedback (note that, it might be necessary to limit the amount of force feedback). But, for larger time delays, reduced fidelity will cause problems. Visual aids like predictive displays will not be applicable as it is virtually impossible to fully model the environment. For larger time delays, supervisory control seems to be the only feasible solution. Under moderate time delays, partial supervisory control, like the one discussed in chapter 6, will be sufficient by avoiding excessive interaction forces.

It is also important to study the kinesthetic perception of the human and to optimize the teleoperation system accordingly. The coupling between the master-slave system can be chosen to minimize perceptual distortion rather than seeking for an ideal response which is marginally stable and practically impossible to achieve. Also some variables of interaction can be amplified to improve sensation of manipulation for better performance. Although there are some studies in literature on human perception in the context of teleoperation [21], there is a lot that needs to be done.

Chapter 6

Hybrid Control

One way to increase safety and performance in telesurgery with time delay is to use a hierarchical control, where the commands of the surgeon transmitted with a time delay are overlaid by a local low level controller which guarantees safety. In this chapter, we will develop a control law using hybrid control design techniques, which can be used as a low level controller to limit interaction forces to guarantee safety under specified disturbances [7].

6.1 Game Theory Approach to Hybrid Control Design

The game theory approach to hybrid control design is briefly summarized here. Interested readers may refer to [5], [26], and [27].

In this approach to hybrid control design, the control problem is formulated as a non-cooperative two player zero-sum dynamical game. Consider a dynamical system:

$$\dot{x} = f(x, u, d, t) \tag{6.1}$$

where $x \in X$ is the state, $u(t) \in U$ is the control input, and $d(t) \in D$ is the disturbance. The game is played between the control input and the disturbance as the opponent. Disturbances can be the (unmodeled) environmental disturbances, control inputs from higher level controllers or behaviors of other agents in a multi-agent system. A cost function, $J(x(0), u, d)$, is defined as the objective of the game, a desired behavior that the controlled dynamical system is desired to satisfy. Suppose $u(\cdot)$ is trying to achieve $J \leq C_1$ while $d(\cdot)$ is trying to maximize it. This game is called a zero-sum game as the win of one player is

the loss of the other. The system is said to admit a saddle solution if there exists a $u^*(t)$ and $d^*(t)$ such that:

$$J(x(0), u^*, d) \leq J(x(0), u^*, d^*) \leq J(x(0), u, d^*) \quad (6.2)$$

If the system admits a saddle solution, the analysis gives the optimum control strategy $u^*(t)$ and a set of “safe” states, S , in which the control can win the game regardless of the disturbance:

$$S = \{x \in X : J(x, u^*, d^*) \leq C_1\} \quad (6.3)$$

Given that the initial condition is in the safe set, the least restrictive control law to achieve $J \leq C_1$ is to use u^* when $x(t)$ is at the boundary of S , without any restriction on the control action when $x(t)$ is inside the safe set. Note that this method gives a switching control law although we started with a continuous time system.

6.2 Controller Design for One DOF Manipulator

In the 1 DOF model of figure 6.1, the manipulator is modeled with the mass m and the actuator force $\tau \in [-\tau_m, \tau_m]$. The contact is modeled with a nonlinear spring, with the force-position characteristic given by

$$F(x) = \begin{cases} 0, & x < 0 \\ kx, & x \geq 0 \end{cases} \quad (6.4)$$

where $k \in [k_{min}, k_{max}]$ is considered as a disturbance. Then, the system is governed by the differential equation

$$m\ddot{x} + k(x)x = \tau(t) \quad (6.5)$$

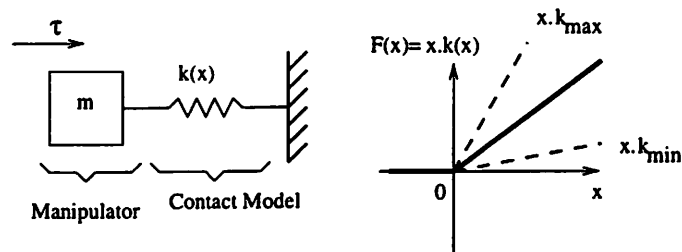


Figure 6.1: 1 DOF contact model

The initial conditions are given as the contact force $F(0) = kx(0)$ and velocity $\dot{x}(0)$ at $t = 0$. Contact force is used here instead of position as one usually has sensors to measure the interaction force, but not the relative position.

The problem is formulated as a two player zero-sum dynamical game between the players $\tau(t)$ and k , which are, respectively, the control and disturbance inputs, with the objective function being the interaction force F .

We start by considering the in-contact problem, *i.e.*, assume that the manipulator is initially in contact, and we want to maintain contact and avoid applying excessive force. In this case, the safety requirement for the control algorithm is specified in terms of the interaction force as

$$F = kx \in [F_{min}, F_{max}] \quad (6.6)$$

The lower bound guarantees maintaining contact, and the upper bound avoids excessive interaction force.

6.2.1 Case 1: $\dot{x}(0) > 0$

In this case, we have the possibility of exceeding the upper limit on the force. First, observe that the maximum force, F_ω , occurs when x is maximum, which is when $\dot{x} = 0$. Here, conservation of energy is used to calculate x_{max} .

The initial energy of the system is:

$$KE_0 + PE_0 = \frac{1}{2}m\dot{x}^2(0) + \frac{1}{2}kx^2(0) = \frac{1}{2}m\dot{x}^2(0) + \frac{1}{2}\frac{F^2(0)}{k} \quad (6.7)$$

The energy input is:

$$E_{in} = \int_{x(0)}^{x_{max}} \tau(x) dx = \tau(\xi)(x_{max} - x(0)) \quad (6.8)$$

for some $\xi \in [x(0), x_{max}]$, where at the last step we used the mean value theorem for integrals, assuming $\tau(t)$ is a continuous function in $t \in [0, t_f]$. The final energy is:

$$KE_f + PE_f = 0 + \frac{1}{2}kx_{max}^2 = \frac{1}{2}\frac{F_\omega^2}{k} \quad (6.9)$$

Solving these equations for F_ω , we find

$$F_\omega = \tau(\xi) + \sqrt{km\dot{x}^2(0) + (\tau(\xi) - F(0))^2} \quad (6.10)$$

Here, we observe that F_ω is monotone in k and $\tau(\xi)$. Then

$$k^* = k_{max}, \quad (6.11)$$

$$\tau^*(t) \equiv -\tau_m \quad (6.12)$$

is the saddle solution.

Then, solving

$$F_\omega^* = -\tau_m + \sqrt{k_{max}m\dot{x}^2(0) + (-\tau_m - F(0))^2} \leq F_{max} \quad (6.13)$$

gives, for $F(0) \leq F_{max}$

$$\dot{x}(0) \leq \sqrt{\frac{(\tau_m + F_{max})^2 - (\tau_m + F(0))^2}{mk_{max}}} \quad (6.14)$$

as the safe set of initial conditions.

6.2.2 Case 2: $\dot{x}(0) < 0$

In this case, we have the possibility of losing contact with the surface, *i.e.* causing the interaction force to drop below F_{min} . Similar to case 1, we observe that the minimum force, F_α , occurs when x is minimum, which is when $\dot{x} = 0$. In the analysis we again use conservation of energy.

The initial energy of the system is the same as case 1:

$$KE_0 + PE_0 = \frac{1}{2}m\dot{x}^2(0) + \frac{1}{2}kx^2(0) = \frac{1}{2}m\dot{x}^2(0) + \frac{1}{2}\frac{F^2(0)}{k} \quad (6.15)$$

The energy input is:

$$E_{in} = \int_{x(0)}^{x_{min}} \tau(x) dx = \tau(\xi)(x_{min} - x(0)) \quad (6.16)$$

for some $\xi \in [x_{min}, x(0)]$, and the final energy is:

$$KE_f + PE_f = 0 + \frac{1}{2}kx_{min}^2 = \frac{1}{2}\frac{F_\alpha^2}{k} \quad (6.17)$$

Solving these equations for F_α , we find

$$F_\alpha = \tau(\xi) - \sqrt{km\dot{x}^2(0) + (\tau(\xi) - F(0))^2} \quad (6.18)$$

which is again monotone in k and $\tau(\xi)$. Then,

$$k^* = k_{max}, \quad (6.19)$$

$$\tau^*(t) \equiv \tau_m \quad (6.20)$$

is the saddle solution.

Then, solving

$$F_\alpha^* = \tau_m - \sqrt{k_{max} m \dot{x}^2(0) + (\tau_m - F(0))^2} \geq F_{min} \quad (6.21)$$

gives, for $F(0) \geq F_{min}$ and $\tau_m \geq F_{min}$

$$\dot{x}(0) \geq -\sqrt{\frac{(\tau_m - F_{min})^2 - (\tau_m - F(0))^2}{mk_{max}}} \quad (6.22)$$

as the safe set of initial conditions.

Putting two conditions together we end up with a “safe” control law such that, as long as

$$\sqrt{\frac{(\tau_m + F_{max})^2 - (\tau_m + F(0))^2}{mk_{max}}} > \dot{x}(0) > -\sqrt{\frac{(\tau_m - F_{min})^2 - (\tau_m - F(0))^2}{mk_{max}}} \quad (6.23)$$

we are free to use any control action, and whenever we are at the upper (lower) boundary we apply $\tau = -\tau_m$ ($\tau = \tau_m$) to guarantee the force condition of equation (6.6), for the specified set of disturbances.

The controller can also be characterized for the free space or approach phase using the previous calculations. During the approach phase, as the manipulator has not yet established contact, $F(0) < F_{min}$, therefore the conditions of equation (6.22) are violated. For free space motion, only the part of the control which deals with F_{max} , given by equation (6.14), is necessary to avoid excessive interaction forces. To maintain contact, the F_{min} part is activated when $F \geq F_{min}$, which will guarantee no loss of contact.

6.2.3 Simulation Results

As a demonstration of the use of this control scheme, consider a mass of $m = 1$ kg controlled by an actuator with a maximum input force of $\tau_m = 80$ N. The wall stiffness is taken to be $k_e = 10^4$ N/m and we wish to maintain the contact force within the range $[F_{min}, F_{max}] = [0.5, 50]$ N.

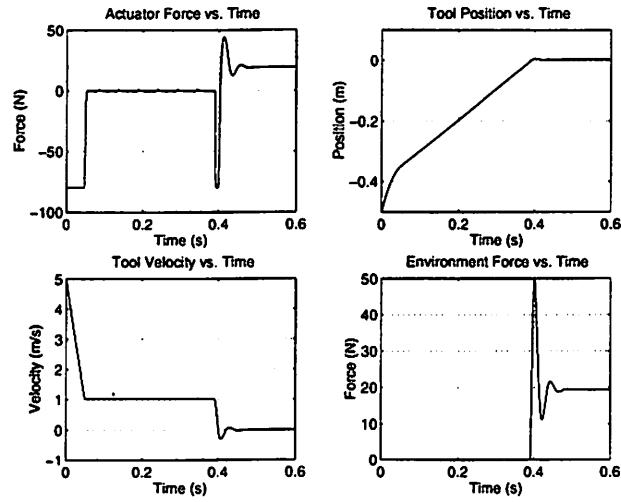


Figure 6.2: Approach phase simulation

In our first simulation, shown in figure 6.2, the mass is initially 0.5 m away from the wall and approaching it with a speed of 5 m/s. Because the mass is in free motion, only the upper bound of (6.23) is activated (the lower bound can only be satisfied during contact). Thus, the actuator applies the maximum negative force, decelerating the mass until it reaches the maximum “approach velocity” which is found by setting $F(0) = 0$ N in equation (6.14) (here, $v_{approach} = 1.02$ m/s). After reaching this velocity, any control is allowed and the one chosen tracks the maximum approach velocity so that contact is made as quickly as possible; as expected, tracking a constant velocity requires negligible force. As soon as contact is made, the actuator applies the maximum negative force again until the mass is in the “safe” region in which an arbitrary controller can be applied for achieving different criteria. For this simulation, a controller was chosen to provide continuity in the actuation forces between the activation of the different regions (*i.e.*, as the velocity approaches the upper bound, $\tau \rightarrow -\tau_m$; similarly, $\tau \rightarrow \tau_m$ as the velocity approaches the lower bound). By choosing this type of continuity in the control, the jerk experienced by the mass is reduced. As can be seen in figure 6.2, the controller performs the desired tasks of bringing the approach velocity to a reasonable value during free motion and maintaining the environment force within the specified bounds during contact, without bouncing.

The second simulation, in figure 6.3, shows the mass being commanded to track a sinusoidal position trajectory while in contact with the surface. In the safe region, a simple PD controller is applied to the mass. As the position increases, the low-level control

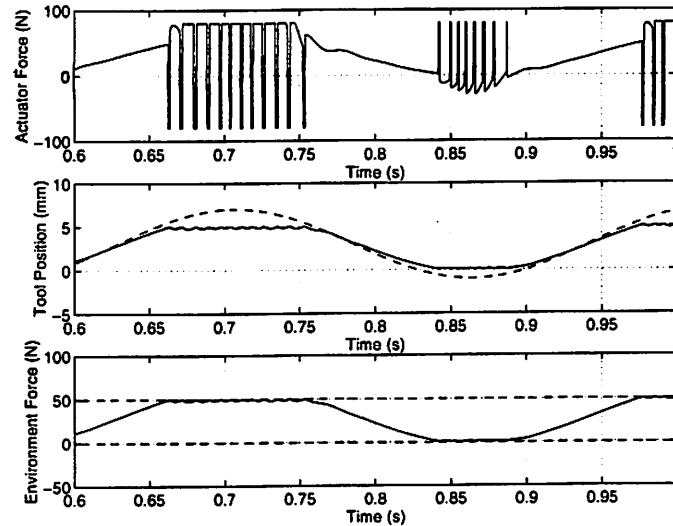


Figure 6.3: In-contact motion simulation

is eventually activated with maximum negative force to prevent exceeding the force safety threshold. After being pushed back into the safe set, the PD controller tries to apply a large positive force because of the deviation from the desired trajectory. As can be seen from the actuator force graph, this cycle repeats itself and there is “chattering” in the actuator control. This chattering becomes more severe as the amplitude of the desired trajectory increases. A similar result occurs when the mass attempts to track the trajectory when it leaves the surface. In this case, the maximum positive force is applied to ensure the minimum force is maintained. Once again, the controller achieves the objectives of tracking a desired trajectory within a safe region and bounding the environment forces at the limits of this region. The plot of the actuator force shows that the price to be paid is a higher actuator bandwidth requirement. If this becomes a problem, the designer has the option to choose a more complicated controller in the safe set such that there is continuity between the different regions.

6.3 Extension to Multi DOF Manipulators

In order to demonstrate the extension of this control scheme to multi DOF manipulators, consider a 2 DOF manipulator with linear joints as an example. Later, we discuss how it can be extended for general manipulators.

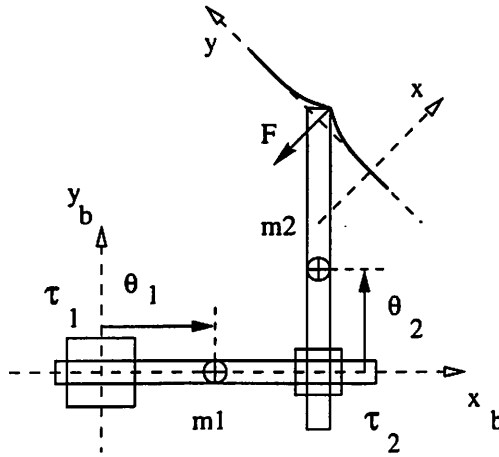


Figure 6.4: 2 DOF manipulator model

The dynamics for the 2 DOF manipulator shown in figure 6.4, in the base coordinate frame (x_b, y_b) , are given by:

$$\begin{bmatrix} m_1 + m_2 & 0 \\ 0 & m_2 \end{bmatrix} \begin{bmatrix} \ddot{\theta}_1 \\ \ddot{\theta}_2 \end{bmatrix} + \underline{F} = \begin{bmatrix} \tau_1 \\ \tau_2 \end{bmatrix} \quad (6.24)$$

where \underline{F} is the interaction force. Assuming we have a frictionless point contact, and modeling the contact force with a spring characterized as in the 1 DOF case, \underline{F} will be normal to the surface and proportional to the normal deformation. If we write the equations in a coordinate frame with the x -axis pointing normally into the surface and centered at the rest position of the surface, we get

$$\tilde{M} \begin{bmatrix} \ddot{x} \\ \ddot{y} \end{bmatrix} + \begin{bmatrix} k(x)x \\ 0 \end{bmatrix} = T \begin{bmatrix} \tau_1 \\ \tau_2 \end{bmatrix} \quad (6.25)$$

$$\begin{bmatrix} \ddot{x} \\ \ddot{y} \end{bmatrix} + \tilde{M}^{-1} \begin{bmatrix} k(x)x \\ 0 \end{bmatrix} = \tilde{M}^{-1} T \begin{bmatrix} \tau_1 \\ \tau_2 \end{bmatrix} \quad (6.26)$$

Here (x, y) denotes the coordinates of the manipulator tip, and $\tilde{M} = TMT^{-1}$ is the transformed inertia matrix. T is the unitary rotation matrix of the transformation from base coordinates to the world coordinates.

As the interaction force is proportional to the x displacement, we are only inter-

ested in the x component of motion:

$$\ddot{x} + \begin{bmatrix} 1 & 0 \end{bmatrix} \tilde{M}^{-1} \begin{bmatrix} k(x)x \\ 0 \end{bmatrix} = \begin{bmatrix} 1 & 0 \end{bmatrix} \tilde{M}^{-1} T \begin{bmatrix} \tau_1 \\ \tau_2 \end{bmatrix} \quad (6.27)$$

This equation has the form:

$$\ddot{x} + \frac{k(x)x}{m} = \frac{1}{m} \tau \quad (6.28)$$

This is exactly the same as the 1 DOF case and the same solution applies. For the free space motion, if there is *a priori* information available about the surface normal direction, it can be used to monitor just one direction of velocity. If not, the control can be applied to the magnitude of velocity, so that F_{max} will not be exceeded in any direction.

The general 6 DOF serial chain manipulator has dynamics of the form:

$$M(\theta)\ddot{\theta} + C(\theta, \dot{\theta})\dot{\theta} + N(\theta, \dot{\theta}) = \tau \quad (6.29)$$

or in the workspace coordinates, (assuming a nonsingular Jacobian):

$$\tilde{M}(\theta)\ddot{x} + \tilde{C}(\theta, \dot{\theta})\dot{x} + \tilde{N}(\theta, \dot{\theta}) = J^{-T}(\theta)\tau \quad (6.30)$$

where θ is the vector of generalized joint variables, τ is the vector of generalized joint forces, and $J(\theta)$ is the Jacobian of the inverse kinematics map.

Because of the nonlinear Coriolis terms and the θ dependence of the mass matrix M , direct application of the game theoretic formulation becomes easily intractable for the general case. However, if some bounds on velocity terms can be applied to infer an upper bound for Coriolis and gravitational terms, which is a reasonable assumption as interaction velocities are supposed to be small, we can use feedback linearization to eliminate these nonlinear effects. Assuming the mass matrix and the Jacobian are approximately constant during interaction:

$$\tau = v + J^T(\tilde{C}(\theta, \dot{\theta})\dot{x} + \tilde{N}(\theta, \dot{\theta})) \quad (6.31)$$

gives (considering interaction with the environment as well)

$$\tilde{M}\ddot{x} + F(x) = J^{-T}v \quad (6.32)$$

We use the upper bounds to modify the available actuator torque after feedback linearization, for example:

$$|v_i| \leq \tau_{i,max} - \sigma_{max}(J^T) \sup(\|\tilde{C}(\theta, \dot{\theta})\dot{x} + \tilde{N}(\theta, \dot{\theta})\|) \quad (6.33)$$

Note that this is a conservative approach, as we are using upper bounds to modify available torques, and also the actuation used for feedback linearization may work against us.

6.4 Discussion

For hard manipulator to hard surface contact, as is pointed out in [28], the duration of collision is very short, and it is very likely that collisions will end before the controller can act because of the unavoidable computational delays. Given this and the limited bandwidth of the actuation, the designed control would be more effective for interaction with a softer environment, like manipulation of soft tissue.

The choice of the controller for the unrestricted region (inside the safe set) is also important for the performance of the controller. If desired a smoothing control law can be used to minimize, if not to completely eliminate, the chattering inherent to the “safe” controller due to its switching nature.

Another application of this control law is to use it as a low level controller to augment other controllers for guaranteed performance. For example, it can be used in a supervisory control algorithm for teleoperation under time delay to guarantee safety.

A more complicated problem currently being studied is the game in which the opponent has the additional ability to control friction. In effect, this results in an uncertainty in the information on the direction of surface normal. The use of this approach to handle controller delay is also an interesting avenue being pursued, with possible applications for modeling computational delays and the limited bandwidth of actuators.

In telesurgery, this control strategy can be used to limit the interaction forces during manipulation, as a low level controller underlying the master-slave control algorithm.

Chapter 7

Visualization Issues in Telesurgery

As discussed above, the main problems that surgeons encounter in laparoscopic surgery are the loss in dexterity as a result of the instruments, and the loss in hand-eye coordination and spatial perception as a result of the imaging system. The former was addressed with the telerobotic manipulator design discussed in chapters 2, 3 and 4. Here, visualization issues will be discussed.

During laparoscopic surgery, the operation region is observed by a laparoscope inserted through one of the incisions. Laparoscopes have fiber-optic channels to carry light to illuminate the abdominal cavity, and lens optics to transmit the images. A CCD camera is connected at the outer end of the laparoscope, and the image is displayed on a high resolution TV display. Laparoscopes have a field of view of typically 76° – 90° . An important feature of laparoscopes is the angle of objective lens relative to the axis of laparoscope. Typical values of angulation are 0° , 30° , 45° and 50° . Although angulated lenses make the use of laparoscope more difficult, it enables them to view behind obstacles. (See figure 7.1).

The obvious problems of the imaging system are:

- Limited field of view of the laparoscope compared to the human eyes.
- Low contrast of the image, which is usually formed with tones of red.
- Reduced depth perception due to monoscopic view.
- Problems with coordination of the primary surgeon with the camera assistant who is acting like the “eyes” of the surgeon. This is more of a problem when an angled scope is used.

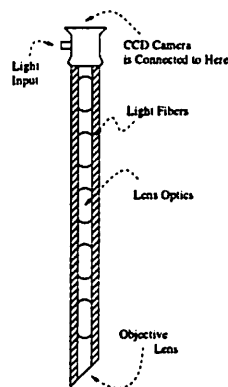


Figure 7.1: Cross-section of a laparoscope

- Lost association between the visual and motor spaces.

Studies carried out with stereo laparoscopes show a limited improvement over monoscopic ones [41] which can explain only half of the difference in performance between the normal vision and laparoscope display. Good contrast is reported to be more important at long working distances. The problem is believed to be a spatial cognition problem, which includes navigation and exploration [40].

Computer vision can be used to improve the imaging system. In the simplest system, camera motion can be controlled under high level commands of the surgeon to track an anatomical landmark or an instrument. In a more sophisticated systems, a 3D stereo view of the scene reconstructed from the image can be displayed to the surgeon using a suitable display device. This way, the surgeon's view would be independent of the constraints of the camera, and the association between the visual and motor spaces can be completely recovered when a telerobotic manipulator is used. The information acquired from other sources, like MRI or ultrasound, can be registered onto the camera or reconstructed display to give surgeon "X-ray eyes." Also in telesurgery under time delay, manipulators can be visually servoed under supervisory control.

7.1 Case Study: 3D Surface Reconstruction from Camera Motion in Laparoscopic Images

In order to understand the feasibility of real-time 3D surface reconstruction in a telesurgery setting, we considered the problem of estimating depth map from camera motion

in laparoscopic images, starting with sample images taken from a videotape of an operation. The camera was not calibrated and there was no information on camera motion. Only some generic information, like field of view and image size, was used. Images used in the study were taken from a laparoscopic indirect hernia repair operation. The frames used were 1 second apart, and taken from a part of the tape where natural motion of body is very small. We neglected this motion for simplicity.

The method used was:

- Sub-sampling of the images (by 1/3) to decrease time complexity
- Calibration of camera — estimation of intrinsic parameters
- Estimation of camera motion — estimation of extrinsic parameters
- Solving stereo correspondence
- Estimation of depth by triangulation

Calibration

The intrinsic parameters of a camera are represented by a matrix:

$$P_{old} = \begin{bmatrix} \alpha_u & 0 & u_0 & 0 \\ 0 & \alpha_v & v_0 & 0 \\ 0 & 0 & 1 & 0 \end{bmatrix} \quad (7.1)$$

where

$$\alpha_u = -fk_u \quad (7.2)$$

$$\alpha_v = -fk_v \quad (7.3)$$

and u_0 and v_0 are the image coordinates of the camera center, k_u and k_v give the aspect ratio of the grid, and f is the focal length of the camera [12]. In normalized coordinates, this matrix has the form

$$P_{new} = \begin{bmatrix} & 0 \\ I_{3 \times 3} & 0 \\ & 0 \end{bmatrix} \quad (7.4)$$

where $P_{new} = HP_{old}$, and H gives the coordinate transformation between image coordinates and the normalized coordinates.

As the laparoscope used was not calibrated, these parameters were not known. For the laparoscope used in the system, k_u and k_v are assumed to be 1, giving a square grid. Focal length of the camera was estimated from the angle of view, which is known to be 68° diagonally, and the unit of measurement was chosen to be the grid size, eliminating the need for scaling. Camera center was recovered from the circular field of view, with the assumption that the field of view actually coincides with the camera center.

Recovering Camera Motion

In order to be able to do triangulation and to use the epipolar constraint in solving stereo correspondence, we need to know the relative motion of the camera between the two frames. If there are 8 or more known corresponding pairs of points in both images, the problem of estimating the camera motion can be imposed as a non-linear optimization problem [12].

In this study, the process of selecting and finding correspondences of these initial sets of points was not automated, although it could be done [49]. Rather, the user interactively selected the rough positions of the corresponding points and then these correspondences were fine matched automatically. Of course this kind of approach is completely unacceptable for on-line or real-time applications. But for the practical case, the laparoscope is to be installed on to a robotic manipulator, in which case the camera motion would be known up to the accuracy of the manipulator. Therefore, this step of recovering camera motion would be unnecessary, only a calibration procedure would be required. But in this feasibility study, recovery of camera motion is essential to continue with the rest of the procedure.

In the project, after the corresponding points were specified and fine matched, we got an initial estimate for translation using part of the eight point algorithm. Then this estimate was used as an initial estimate for the non-linear optimization using Longuet-Higgins (LH) criterion. In LH method [12] the cost

$$LH(R, t) = \sum_i (m_i \cdot (t \wedge R m'_i))^2 \quad (7.5)$$

is minimized over q and t , where q is the quaternion representing the rotation R , and t is the translation, subject to the constraints $\|q\| = 1$ and $\|t\| = 1$. m_i and m'_i are the normalized coordinates of the corresponding points in the two images.

Solving Stereo Correspondence

This part is essentially an implementation of a stereo algorithm. In the chosen algorithm, epipolar, ordering and smoothness constraints are used (Refer to [12] for details of these constraints). As the environment being observed is the intra-abdominal cavity, which is essentially composed of smooth surfaces, ordering and smoothness constraints are completely acceptable.

The algorithm implemented is a correlation based stereo algorithm described in [13]. The correlation measure used is $\langle I_1, I_2 \rangle / (||I_1|| ||I_2||)$, where I_1 and I_2 are the intensities of a neighborhood of points around the examined points from the first and second images, respectively. As the recovered camera motion was not very reliable the search is performed over a bar of $2 \times 4 + 1$ pixels wide around the epipolar line, to increase accuracy. Also, the correspondence is validated by performing the search again, this time from second image to the first, and accepting the correspondence only if the second match gives the original point on the first image. The aim is to calculate the disparity accurately, in the expense of getting a sparse map.

Implementation Details

The stereo algorithm had the longest execution time among the implemented steps. The current version of the stereo algorithm, implemented using MATLAB version 4.2c and Image Processing Toolbox version 1.0b, processes the two images of size 162×214 in about 2 hours on an SGI Indigo 2 workstation.

Results and Discussion

Estimated epipolar lines of points used in camera motion estimation, and for some test points are shown in figures 7.2 and 7.3 respectively. Recovered depth map of the first image is shown in figure 7.4.

In the results given above, correspondence was calculated over a relatively sparse set of points in order to decrease the time complexity of the algorithm. Considering the smoothness constraint, the depth is interpolated from this sparse set of calculations. The disadvantage of this approach is the decreased accuracy. Also the algorithm did not perform very well at parts of the image where illumination is changing significantly. This is a result of the choice of correlation measure, and therefore was expected. A better correlation

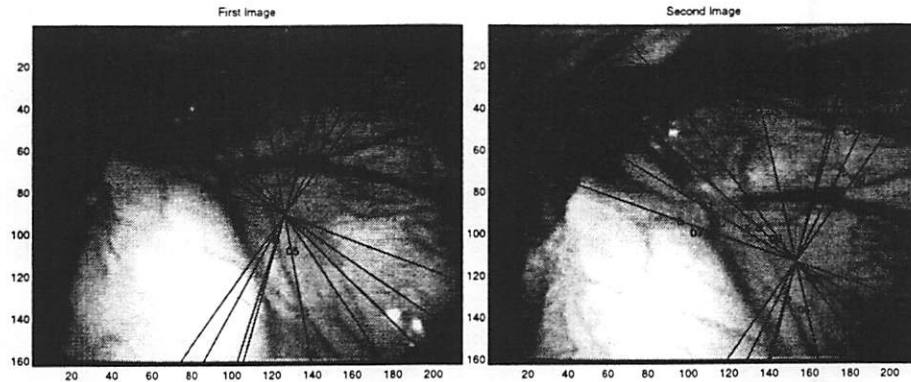


Figure 7.2: Epipolar lines for calculation points

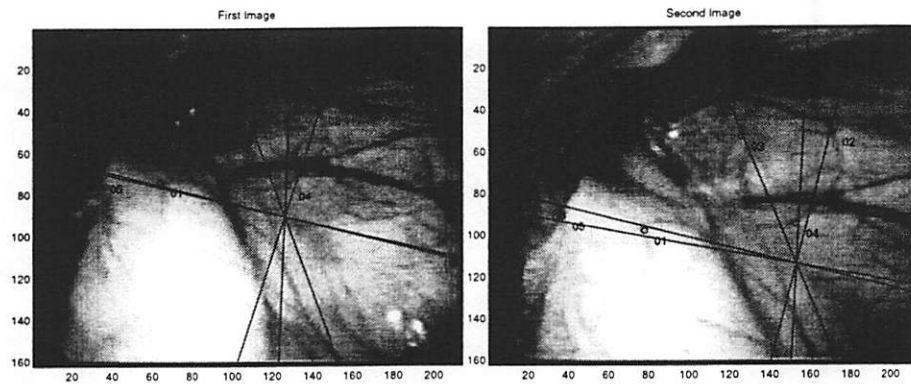


Figure 7.3: Epipolar lines for test points

technique (like normalized cross correlation - NCCR) would yield better results at the expense of increased running time.

Another problem in correspondence is that some points on the image might not have a corresponding point on the other image. The implemented algorithm can cope with this successfully, as a result of the validation of correspondences, as it can be seen from the results.

In the real application, calibration step can essentially be eliminated completely by using a calibrated laparoscope, in which case accurate information on camera parameters would be available. Also, as the camera will be mounted on a 4 DOF robotic manipulator, camera motion estimation step can be eliminated as well, while accurate motion information will be available. Use of a better correlation criteria, like NCCR, is necessary because of the environment being observed. The lack of texture in the environment should also be

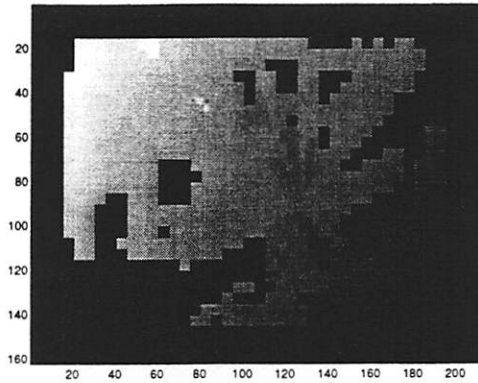


Figure 7.4: Calculated depth map

considered during stereo matching phase. The self motion of the body needs to be modeled and included in the algorithm as well as the deformations resulting from the manipulation of tissue. Implementation on a specialized parallel platform, like in [13], might be necessary for real-time operation.

Chapter 8

Conclusion and Future Directions

This study addressed the various aspects of telesurgery. We have first introduced the Berkeley/UCSF Telesurgical Workstation, a master-slave telerobotic system designed considering the special requirements of minimally invasive telesurgery, followed by its kinematic analysis, and control. In the second part, conceptual and future issues on telesurgery are studied in detail, including discussions on teleoperation, hybrid control and visualization.

Discussions on teleoperation first pointed out the fidelity-stability trade-off in teleoperation systems, and discussed its implications for telesurgery. Then the control algorithms present in the literature were compared in the context of telesurgery, and the requirements and critical factors of telesurgery are identified.

Hierarchical control was proposed to increase the safety and performance in telesurgery. Hybrid control techniques were used to design a low-level controller for the telesurgical robot, the least restrictive control law to limit the interaction forces for guaranteed safe operation.

The visualization section discussed the general problems of the display system used in laparoscopic surgery, and proposed ways to overcome these problem, with a case study on 3D surface reconstruction from camera motion in laparoscopic images.

Directions for Future Work

The future work can be pointed out in two directions. For the Berkeley/UCSF Telesurgical Workstation, the proposed control algorithm needs to be implemented, with

the force feedback and safety monitor, followed by experimental studies to further analyze the effectiveness of the robot and the control.

On the conceptual side, the kinesthetic perception of the human should be experimentally studied to further identify the design goals for an effective teleoperation system design. Also further experimental and theoretical studies are necessary to compare various robot and control designs, under non-ideal conditions, especially in the context of telesurgery.

The low-level controller designed using hybrid control techniques needs to be efficiently generalized to 6 DOF, and to the cases with actuator time delay and environment friction.

For visualization, the implemented 3D surface reconstruction algorithm needs to be improved, based on the results obtained from the current version. Also, the problem of registration of information obtained from various sources should be pursued as it has important applications.

Bibliography

- [1] R. J. Anderson and M. W. Spong. Bilateral Control of Teleoperators with Time Delay. *IEEE Transaction on Automatic Control*, 34(5):494–501, May 1989.
- [2] R. J. Anderson and M. W. Spong. Asymptotic Stability for Force Reflecting Teleoperators with Time Delay. *International Journal of Robotics Research*, 11(2):153–148, April 1992.
- [3] F. Arai, M. Tanimoto, T. Fukuda, K. Shimojima, H. Matsuura, and M. Negoro. Multimedia Tele-surgery Using High Speed Optical Fiber Network and Its Applications to Intravascular Nerosurgery — System Configuration and Computer Networked Implementation. In *Proceedings of the IEEE International Conference on Robotics and Automation*, volume 1, pages 878–883, 1996.
- [4] T. Arai, S. Hashino, E. Nakano, and K. Tani. Advanced Teleoperation with Configuration Differing Bilateral Master-Slave System. In *Robotics Research, the Fourth International Symposium*, pages 163–170, 1988.
- [5] T. Başar and G. J. Olsder. *Dynamic Non-cooperative Game Theory*. Academic Press, second edition, 1995.
- [6] T. L. Brooks. Telerobotic Response Requirements. In *Proceedings of the IEEE International Conference on Systems, Man and Cybernetics*, pages 113–120, 1990.
- [7] M. C. Çavuşoğlu, J. Yan, and S. S. Sastry. A Hybrid System Approach to Contact Stability and Force Control in Robotic Manipulators. In *Proceedings of the 12th IEEE International Symposium on Intelligent Control*, 1997.
- [8] M. Cohn, L. S. Crawford, J. M. Wendlandt, and S. S. Sastry. Surgical Applications of Milli-Robots. *Journal of Robotics Systems*, 12(6):401–416, June 1995.

- [9] M. B. Cohn, M. Lam, and R. S. Fearing. Tactile Feedback for Teleoperation. In *Proceedings of the SPIE*, volume 1833, pages 240–254, 1993.
- [10] J. E. Colgate. Robust Impedance Shaping Telemanipulation. *IEEE Transactions on Robotics and Automation*, 9(4):374–384, August 1993.
- [11] H. Das, H. Zak, W. S. Kim, A. K. Bejczy, and P. S. Schenker. Operator Performance with Alternative Manual Control Modes in Teleoperation. *Presence*, 1(2):201–218, Spring 1992.
- [12] O. Faugeras. *Three Dimensional Computer Vision*. MIT Press, 1993. Chapters 3, 6 and 7.
- [13] O. Faugeras and et. al. Real Time Correlation-Based Stereo Algorithm, Implementation and Applications. Technical Report INRIA Research Report No 2013, INRIA Sophia-Antipolis, France, 1993.
- [14] K. Furuta, K. Kosuge, Y. Shiote, and H. Hatano. Master-Slave Manipulator Based on Virtual Internal Model Following Control Concept. In *Proceedings of the IEEE International Conference on Robotics and Automation*, pages 567–572, 1987.
- [15] E. Graves. *Vital and Health Statistics*. Data from the National Health Survey No. 122. U.S. Department of Health and Human Services, Hyattsville, MD, 1993.
- [16] B. L. Gray and R. S. Fearing. A Surface Micromachined Microtactile Sensor Array. In *Proceedings of the IEEE International Conference on Robotics and Automation*, volume 1, pages 1–6, 1996.
- [17] B. Hannaford. A Design Framework for Teleoperators with Kinesthetic Feedback. *IEEE Transactions on Robotics and Automation*, pages 426–434, August 1989.
- [18] B. Hannaford. Stability and Performance Tradeoffs in Bi-Lateral Telemanipulation. In *Proceedings of the IEEE International Conference on Robotics and Automation*, pages 1764–1767, 1989.
- [19] B. Hannaford, L. Wood, D. A. McAfee, and H. Zak. Performance Evaluation of a Six-Axis Generalized Force-Reflecting Teleoperator. *IEEE Transactions on System, Man, and Cybernetics*, 21(3):620–633, May/June 1991.

- [20] J. W. Hill, P. S. Green, J. F. Jensen, Y. Gorf, and A. S. Shah. Telepresence Surgery Demonstration System. In *Proceedings of the IEEE International Conference on Robotics and Automation*, pages 2302–2307, 1994.
- [21] L. A. Jones and I. W. Hunter. Analysis of the Human Operator Controlling a Teleoperated Microsurgical Robot. In *Proceedings of 6th IFAC/IFIP/IFORS/IEA Symposium on Analysis, Design and Evaluation of Man-Machine Systems*, pages 593–597, 1995.
- [22] W. S. Kim, B. Hannaford, and A. K. Bejczy. Force-Reflection and Shared Compliant Control in Operating Telemanipulators with Time Delay. *IEEE Transactions on Robotics and Automation*, 8(2):176–185, April 1992.
- [23] S. Lavallée, J. Troccaz, L. Gabarit, P. Cinquin, A. L. Benabid, and D. Hoffmann. Image Guided Operating Robot: A Clinical Application in Stereotactic Neurosurgery. In R. H. Taylor, S. Lavallée, G. Burdea, and R. Mösges, editors, *Computer Integrated Surgery: Technology and Clinical Applications*. MIT Press, 1995.
- [24] C. A. Lawn and B. Hannaford. Performance Testing of Passive Communication and Control in Teleoperation with Time Delay. In *Proceedings of the IEEE International Conference on Robotics and Automation*, pages 776–783, 1993.
- [25] D. A. Lawrence. Stability and Transparency in Bilateral Teleoperation. *IEEE Transactions on Robotics and Automation*, 9(5):624–637, October 1993.
- [26] J. Lewin. *Differential Games*. Springer-Verlag, 1994.
- [27] J. Lygeros, D. N. Godbole, and S. S. Sastry. A Game Theoretic Approach to Hybrid System Design. Technical report, University of California, Berkeley, 1995.
- [28] J. K. Mills. Manipulator Transition to and from Contact Tasks: A Discontinuous Control Approach. In *Proceedings of the IEEE International Conference on Robotics and Automation*, pages 440–446, 1990.
- [29] R. M. Murray, Z. Li, and S. S. Sastry. *A Mathematical Introduction to Robotic Manipulation*. CRC Press, Inc., 1994.
- [30] G. Niemeyer and J. J. E. Slotine. Stable Adaptive Teleoperation. *IEEE Journal of Oceanic Engineering*, 16(1):152–162, January 1991.

- [31] G. J. Raju, G. C. Verghese, and T. B. Sheridan. Design Issues in 2-port Network Models of Bilateral Remote Manipulation. In *Proceedings of the IEEE International Conference on Robotics and Automation*, pages 1316–1321, 1989.
- [32] A. Rovetta, R. Sala, X. Wen, and A. Togno. Remote Control in Telerobotic Surgery. *IEEE Transactions on Systems, Man, and Cybernetics—Part A: Systems and Humans*, 26(4):438–443, July 1996.
- [33] D. N. Roy. *Applied Fluid Mechanics*. Ellis Horwood Limited, 1988.
- [34] S. S. Sastry, M. Cohn, and F. Tendick. Millirobotics for Remote, Minimally-Invasive Surgery. *Journal of Robotics Systems*, to appear in 1997.
- [35] T. B. Sheridan. *Telerobotics, Automation, and Human Supervisory Control*. MIT Press, 1992.
- [36] T. B. Sheridan. Space Teleoperation Through Time Delay: Review and Prognosis. *IEEE Transactions on Robotics and Automation*, 9(5):592–606, October 1993.
- [37] P. S. Schenker, H. Das, and T. R. Ohm. A New Robot for High Dexterity Microsurgery. In N. Ayache, editor, *Computer Vision, Virtual Reality and Robotics in Medicine. First International Conference, CVRMed'95. Proceedings.*, pages 115–122, Berlin, Germany, 1995. Springer-Verlag.
- [38] R. H. Taylor, J. Funda, B. Eldridge, S. Gomory, K. Gruben, D. LaRose, M. Talamini, L. Kavoussi, and J. Anderson. A Telerobotics Assistant for Laparoscopic Surgery. *IEEE Engineering in Medicine and Biology Magazine.*, 14(3):279–288, May–June 1995.
- [39] R. H. Taylor, B. D. Mittelstadt, H. A. Paul, W. Hanson, P. Kazanzides, and et. al. An Image-Directed Robotics System for Precise Orthopaedic Surgery. *IEEE Transactions on Robotics and Automation*, 10(3):261–275, June 1994.
- [40] F. Tendick. Personal Communication, 1997.
- [41] F. Tendick, S. Bhojru, and L. Way. Comparison of laparoscopic imaging systems and conditions using a knot tying task. *Journal of Image Guided Surgery*, 2(1), 1996.

- [42] R. Tombropoulos, A. Schweikard, J. C. Latombe, and J. R. Adler. Treatment Planning for Image-Guided Robotic Radiosurgery. In N. Ayache, editor, *Computer Vision, Virtual Reality and Robotics in Medicine. First International Conference, CVRMed '95. Proceedings.*, pages 131–137, Berlin, Germany, 1995. Springer-Verlag.
- [43] L. W. Way, S. Bhojrul, and T. Mori, editors. *Fundamentals of Laparoscopic Surgery.* Churchill Livingstone, 1995.
- [44] J. Wendlandt. Milli Robotics for Endoscopy. Memo M94/7, UC Berkley ERL, January 1994.
- [45] J. Wendlandt and S. S. Sastry. Design and Control of a Simplified Stewart Platform for Endoscopy. In *Proceedings of the IEEE Conference on Decision and Control*, volume 1, pages 357–362, 1994.
- [46] J. Yan and S. E. Salcudean. Teleoperation Controller Design Using H-infinity Optimization with Application to Motion-Scaling. *IEEE Transactions on Control Systems Technology*, 4(3):244–258, May 1996.
- [47] Y. Yokokohji and T. Yoshikawa. Bilateral Control of Master-Slave Manipulators for Ideal Kinesthetic Coupling—Formulation and Experiment. In *Proceedings of the IEEE International Conference on Robotics and Automation*, pages 849–858, 1992.
- [48] Y. Yokokohji and T. Yoshikawa. Bilateral Control of Master-Slave Manipulators for Ideal Kinesthetic Coupling—Formulation and Experiment. *IEEE Transactions on Robotics and Automation*, pages 605–6–20, October 1994.
- [49] Z. Zhang and et. al. A Robust Technique for Matching Two Uncalibrated Images Through Recovery of the Unknown Epipolar Geometry. Technical Report INRIA Research Report No 2273, INRIA Sophia-Antipolis, France, May 1994.